energies

MDPI

Article

A Novel Control Algorithm Design for Hybrid Electric Vehicles Considering Energy Consumption and Emission Performance

Yuan Qiao [1], Yizhou Song [1,2] and Kaisheng Huang [1,2,3,*]

1 State Key Laboratory of Automotive Safety and Energy, School of Vehicle and Mobility, Tsinghua University, Beijing 100084, China
2 The Joint Laboratory for Internet of Vehicles, Ministry of Education - China Mobile Communications Corporation, Beijing 100084, China
3 Collaborative Innovation Center of Electric Vehicles in Beijing, Beijing 100081, China
* Correspondence: huangks@tsinghua.edu.cn; Tel.: +86-138-0123-7852

Received: 14 June 2019; Accepted: 12 July 2019; Published: 15 July 2019

Abstract: Under the severe challenge of increasingly stringent emission regulations and constantly improving fuel economy requirements, hybrid electric vehicles (HEVs) have attracted widespread attention in the auto industry as a practicable technical route of green vehicles. To address the considerations on energy consumption and emission performance simultaneously, a novel control algorithm design is proposed for the energy management system (EMS) of HEVs. First, energy consumption of the investigated P3 HEV powertrain is determined based on bench test data. Second, crucial performance indicators of NOx and particle emissions, prior to a catalytic converter, are also measured and processed as a prerequisite. A comprehensive objective function is established on the grounds of the Equivalent Consumption Minimization Strategy (ECMS) and corresponding simulation models are constructed in MATLAB/SIMULINK. Subsequently, the control algorithm is validated against the simulation results predicated on the Worldwide-Harmonized Light-Vehicle Test Procedure (WLTP).Integrated research contents include: (1) The searching process aimed at the optimal solution of the pre-established multi-parameter objective function is thoroughly investigated; (2) the impacts of weighting coefficients pertaining to two exhaust pollutants upon the specific configurations of the proposed control algorithm are discussed in detail; and (3) the comparison analysis of the simulation results obtained from ECMS and classical Dynamic Programming (DP), respectively, is performed.

Keywords: hybrid electric vehicles; control algorithm design; energy consumption; emission performance

1. Introduction

Human beings have used fossil fuels in large quantities since the first Industrial Revolution. The discovery and exploitation of petroleum has significantly promoted the development of internal combustion engines and fuel vehicles [1–3]. Nevertheless, conventional vehicles with high fuel consumption and massive exhaust emissions have become more and more subject to fierce criticism due to serious energy shortage and potential environmental pollution problems [4,5]. Pressured by increasingly stringent emission regulations and constantly improving fuel economy requirements, green vehicles including hybrid electric vehicles (HEVs), plug-in hybrid electric vehicles (PHEVs), battery electric vehicles (BEVs), and fuel cell electric vehicles (FCEVs) have attracted attention from the entire automobile industry [6,7]. Considering these different technical routes, the so-called range anxiety problem and the perceived inconvenience of charging vehicles set barriers to the widespread acceptance of PHEVs and BEVs [8,9]. Additionally, the inadequacies of existing hydrogen production, storage, and transportation technology, the poor infrastructure construction of hydrogen refueling station as well as soaring manufacturing costs have always been the biggest obstacles restricting the large-scale industrialization of FCEVs [10]. In contrast, HEVs display unique advantages in structural compatibility and control system complexity without suffering from the severe capacity fading of power batteries. Consisting of an engine, most of the time a motor and a battery, HEVs combine the advantages of conventional fuel-powered vehicles and pure electric vehicles, which makes HEVs a practicable technical scheme and consequently gives rise to its prosperity in the field of both academic research and industrial application [11,12].

With respect to the core technologies of HEVs development, energy management system (EMS) undoubtedly occupies an important position. For the purpose of realizing better fuel economy and lower power consumption, EMS is generally designed to locate the operating points of a vehicle engine in the optimal efficiency region [13]. Integrated EMS is capable of making significant difference in HEVs overall performance improvement. Therefore, the hierarchical control architecture and the concrete control strategy of EMS have been considered as a research hotspot by many corporations and institutes, especially in Europe, Japan, and the United States [11,14].

Homchaudhuri et al. presented a hierarchical control strategy for connected HEVs in urban road conditions. Both higher level controller and lower level controller solved problems focused on fuel efficiency and energy management. Information about driving conditions was captured and made full use of. First, traffic light information was utilized through vehicle to infrastructure (V2I) communication. Secondly, state information of the vehicles in its near neighborhood was utilized via vehicle to vehicle (V2V) communication [15]. Zhang et al. quantitatively analyzed and evaluated current research status of energy management strategies for HEVs based on bibliometrics for the first time and put forward the emphasis and orientation of future study which aimed at promoting the development of a simple and practical energy management controller with low cost and high performance for HEVs [16]. Bayindir et al. proposed an overview of HEVs with a focus on hybrid configurations, energy management strategies, and electronic control units, clearly emphasizing the advantages and disadvantages of each configuration [17]. Yi et al. introduced a novel architecture of hybrid electric powertrain systems which suppressed torque fluctuations and carried out the functionality of hybrid driving. A model for this new powertrain was established and a specially designed ruled-based multi-state controller was included to achieve control and enhance fuel economy [18]. Shabbir and Evangelou put forward a real-time control strategy called supervisory control system (SCS) to maximize HEV powertrain efficiency. It was tested and benchmarked against two conventional control strategies in a high-fidelity vehicle model, representing a series HEV. Extensive simulation results were presented for repeated cycles of a diverse range of standard driving cycles, showing significant improvements in fuel economy (up to 20%) and less aggressive use of the battery [19].

Additionally, Model Predictive Control (MPC) should not be neglected as a research hotspot, as it is an online strategy able to manage fuel consumption, battery aging, and overall cost of energy simultaneously. Sockeel et al. provided a Pareto-front analysis of the objective function, taking into account the equivalent fuel consumption and the battery aging for PHEVs in the charge sustaining (CS) mode [20]. Furthermore, the concrete influences of how to estimate the state of charge on MPC performance with respect to equivalent fuel consumption and battery capacity fades were also thoroughly investigated [21]. Prevailing power management strategy (PMS) utilized in HEVs were summarized by Huang et al. from a comprehensive perspective [22]. Based on detailed comparison, they initially attached significant importance to MPC based strategies. Di Cairano et al. presented a novel method for driver-aware vehicle control based on stochastic model predictive control with learning (SMPCL) and backed up it with experimental validation [23]. A MPC torque-split strategy fully considering corresponding diesel engine transient characteristics was proposed by Yan et al. for the first time. Simulation research based on an HEV model with actual system parameters and an experimentally validated diesel-engine model indicated that the proposed MPC supervisory strategy considering diesel engine transient characteristics possessed superior equivalent fuel efficiency while maintaining HEV driving performance [24]. Rashid and Minh built up a typical model of a parallel HEV and developed model predictive controllers for this model to control the speeds and torques for fast clutch engagement with high driving comfort and low jerk. Some modified algorithms for model predictive controllers were also studied to improve their ability to track the desired speed set points, subject to input and output constraints [25]. Xiang et al. proposed a real time EMS for a dual-mode power-split HEV in order to improve the fuel economy and maintain proper battery's state of charge while satisfying all the constraints and the driving demands. The EMS employed a cascaded control concept including a velocity predictor, a master controller and a slave controller. The velocity predictor was proposed based on radial basis function neural network and forward dynamic programming was employed in nonlinear model predictive control to improve efficiency [26].

In general, HEVs are one of the most promising solutions for reducing fuel consumption and exhaust emissions [27]. Furthermore, how to optimize the specific control algorithm for EMS and obtain a more comprehensive power allocation scheme is one of the major topics to be investigated in this field. Unfortunately, most previous studies addressed the concerns including fuel economy, power performance, and overall powertrain efficiency. In particular, few studies, to our knowledge, have considered the impacts of exhaust pollutants and put as much emphasis on emission reduction as on energy conservation. Apparently, the EMS, which only considers fuel economy and power performance, cannot meet the tougher requirements on environmental influence. To illuminate this uncharted area, a novel control algorithm design for HEVs considering both energy consumption and emission performance is proposed. A combined objective function is established on the grounds of the Equivalent Consumption Minimization Strategy (ECMS) [28,29]. Taking into account the indicators of both energy consumption and emission performance, we adopt a normalization method in purpose to eliminate the adverse effects caused by different dimensions. The emission data of NOx and particle are measured and processed as a prerequisite for subsequent control algorithm design. Corresponding emission model is carefully selected and validated against the experimental data to guarantee its accuracy. Associated with the established mathematical model of multi-objective optimization, a simulation model is built in MATLAB/SIMULINK accordingly. First, the proposed optimization method is tested against the measured data based on the Worldwide-Harmonized Light-Vehicle Test Procedure (WLTP). Second, the impacts of weighting coefficients pertaining to different kinds of pollutants upon the final results are discussed in detail. By comparing the optimization results with that obtained by classical Dynamic Programming (DP), the feasibility and accuracy of the proposed control algorithm are demonstrated.

2. Energy Consumption and Emission Performance Indicators Modeling

2.1. HEV Powertrain Configuration

In terms of existing HEVs, parallel powertrain architecture is broadly applied due to its unique advantages in control complexity [18,30,31]. A P3 HEV oriented at both Europe and China auto market is set as the research focus of this paper with its vehicle model constructed in MATLAB/SIMULINK environment. P3 refers to a kind of HEV powertrain structure in which the motor is located at the output of gearbox. Figure 1 displays the structure of the investigated P3 HEV powertrain. As shown in Figure 1, high voltage (HV) battery and gasoline engine conspire to provide the power needed for driving the vehicle. Specifications of the gasoline engine are presented in Table 1.

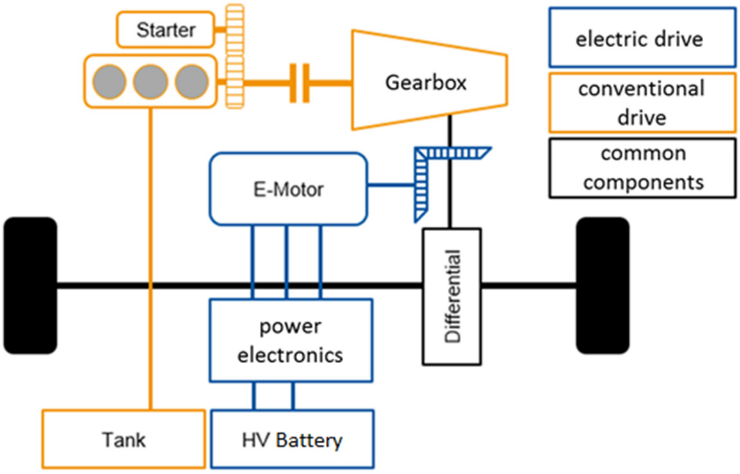

Figure 1. Structure of the investigated P3 hybrid electric vehicles (HEV) powertrain.

Table 1. Gasoline engine specifications.

Parameters	Value
Type	L4
Displacement	1498 cm^3
Bore	74.5 mm
Stroke	85.9 mm
Bore/stroke ratio	0.867
Compress ratio	12.5
Maximum power	96 kW
Maximum torque	200 N·m
Intake valve opening event	150 °CA
Exhaust valve opening event	180 °CA
Fuel	ROZ95 E10

2.2. *Quadratic Polynomial Fitting of Consumed Power*

The overall consumed energy of the investigated P3 HEV powertrain is composed of two parts: The chemical energy contained in fuel burned in the internal combustion engine (ICE) and the electric energy supplied to the motor. The former is denoted as chemical energy consumed power and the latter is denoted as electric energy consumed power. A large number of bench tests are conducted in purpose to obtain a precise estimation of the functional relationship between output torque and the consumed power. As displayed in Figure 2, experimental data are marked as cross dots with different colors indicating different engine speed. It can be obviously observed that chemical energy consumed power is changed along with engine torque content in a manner of approximate quadratic function regularity. Similarly, it can be derived that there exists a quadratic function between motor torque and electric energy consumed power as shown in Figure 3. It is important to note that motor torque and electric energy consumed power can be simultaneously negative under the circumstance that the E-Motor in Figure 1 acts as a generator. On this condition, the HV battery will be charged and electric energy consumed power actually turns into charging power. As a consequence, the quadratic curves of the motor can be divided into two central-symmetric parts with zero as a demarcation point.

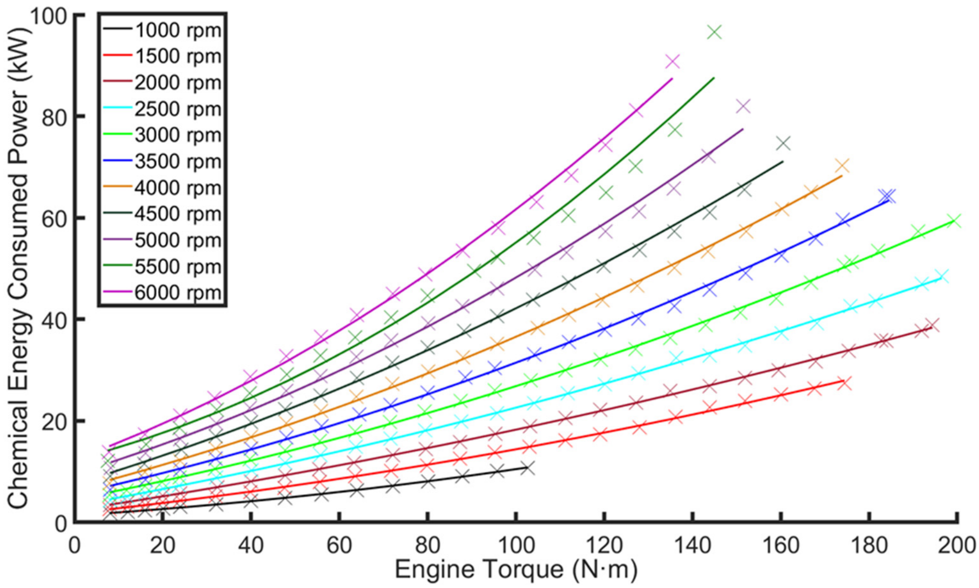

Figure 2. Fitting results of the chemical energy consumed power.

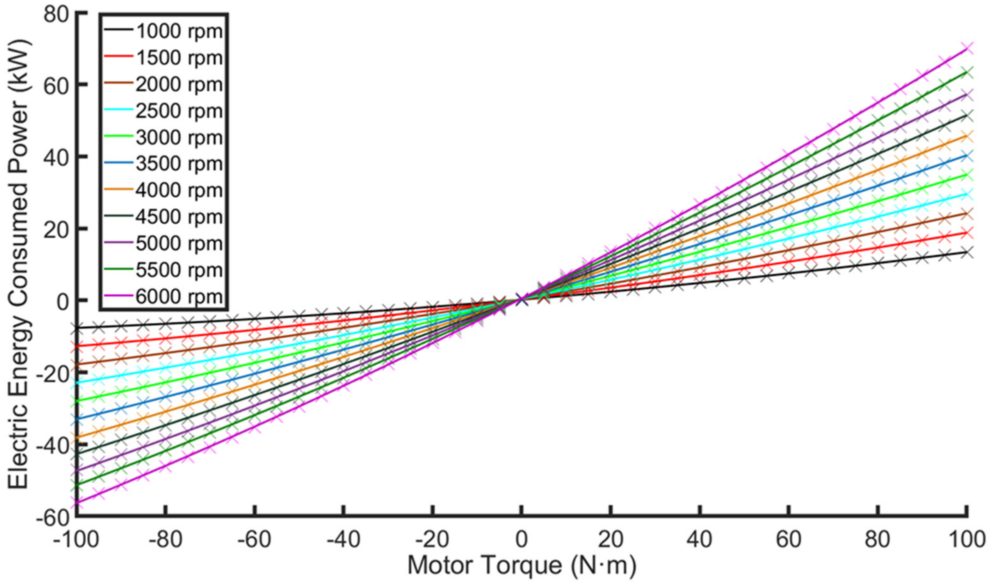

Figure 3. Fitting results of the electric energy consumed power.

Based on the experimental data, quadratic polynomial fitting is introduced into describing the relationship between the consumed power and interrelated output torque. The equation is as follows:

$$P_{EC} = p_{1,EC} + p_{2,EC}M_{EC} + p_{3,EC}M_{EC}^2 \tag{1}$$

where P_{EC} is one of these two energy consumed power mentioned above, M_{EC} is the corresponding output torque (engine torque or motor torque), and $p_{1,EC}$, $p_{2,EC}$, and $p_{3,EC}$ are fitting coefficients. It should be noted that with respect to the electric energy consumed power, there exists two different quadratic function expressions over full operating range. Alternatively, a piecewise function can be employed to integrate these two segments with zero as a demarcation point as mentioned above.

2.3. Quadratic Polynomial Fitting of Emission Data

Apart from addressing the concerns about energy consumption, it is equally important to work out emissions accurately and rapidly for the purpose of realizing the subsequent optimization of emission performance and energy consumption simultaneously. Table 2 displays the vital modeling components of several mainstream emissions modeling methodologies [32,33]:

Table 2. Characteristics of several mainstream emission models.

Emission Models	Vehicle Test Procedure	Emission Representation	Vehicle Activity Factors
Parameterized Physical Model	short driving cycle to determine key parameters	parameterized analytical representation	second-by-second profile and/or parameterized trip characteristics
Velocity-Acceleration Matrix Model	second-by-second emissions testing for all modes	average emissions for each mode of velocity-acceleration	time spent in velocity-acceleration matrix
Emission Mapping Model	second-by-second emissions testing	emissions map for all modes of engine power and speed	engine power and speed (must be translated from second-by-second velocity profile)

Among these models above, the Parameterized Physical Model calculates emissions according to the fuel consumption rate [33]:

$$ER = FR\cdot\left(\frac{g_{emissions}}{g_{fuel}}\right)\cdot CPF \tag{2}$$

where ER is specific emission rate, FR is fuel consumption rate, $g_{emissions}$ is the mass of engine-out emissions, and g_{fuel} is the mass of consumed fuel. CPF is defined as catalyst pass fraction, which indicates the proportion of emissions discharged through the tailpipe. CPF is usually a function primarily of air/fuel ratio (A/F) and engine-out emissions. Additionally, Equation (2) can be approximately estimated is shown as follows:

$$ER \approx \left[C_0\cdot\left(1-\phi^{-1}\right)+C_1\right]\cdot FR \tag{3}$$

where C_0 is the weigh coefficient and approximately set as 3.6, ϕ is the fuel/air equivalence ratio and C_1 is defined as the emission index coefficient (engine-out emissions in g/s divided by fuel consumption rate in g/s), which can be measured under stoichiometric combustion condition. Further, the equation for calculating CPF is:

$$CPF = 1-\Gamma\cdot\exp\left[\left(-C_F-C_M\cdot\left(1-\phi^{-1}\right)\right)\cdot FR\right] \tag{4}$$

where Γ is the maximum catalyst carbon monoxide (CO) or hydrocarbon (HC) efficiency, C_F is the stoichiometric CPF coefficient calibrated based on the low power Federal Test Procedure (FTP) Bag 2 cycle, and C_M is the enrichment CPF coefficient calibrated based on the 1st Version of the Modal Emissions (MEC01) cycle.

Both the Velocity-Acceleration Matrix Model and the Emission Mapping Model calculate the emissions through map look-up. The difference between them is that velocity and acceleration are defined as independent variables in the first map while their counterparts in the second map are engine power and speed. Furthermore, some regression models have been employed by previous researchers to simplify the calculation mainly based on comparatively sophisticated map look-up process. For the Velocity-Acceleration Matrix Model, the engine-out emissions can be calculated as shown [34,35]:

$$ER = \left(a_1+b_1v+c_1v^2\right)+\left(a_2+b_2v+c_2v^2\right)a+\left(a_3+b_3v+c_3v^2\right)a^2 \tag{5}$$

$$v = \frac{n}{i_0 i_g}\cdot 2\pi R \tag{6}$$

$$a = \frac{\frac{(M_{ICE}i_g+M_{MOT}i_m)i_0}{R}-\frac{1}{2}c_d A\rho_{air}v^2-mgf_r}{m} \tag{7}$$

where $a_1, a_2, a_3, b_1, b_2, b_3, c_1, c_2, c_3$ are regression coefficients, v is vehicle velocity, a is vehicle acceleration, n is engine speed, i_0 is the reduction gear ratio of main decelerator, i_g is the transmission ratio of gearbox, R is the radius of wheel, M_{ICE} is engine torque, M_{MOT} is motor torque, i_m is the transmission ratio of motor gearbox, c_d is aerodynamic drag coefficient, A is cross-sectional area, ρ_{air} is the mass density of ambient air, m is entire vehicle weight, and f_r is rolling resistance coefficient. As for the Emission Mapping Model, v and a in Equation (5) are replaced with engine power and speed, respectively. In addition, Asher et al. have established an emission model based on artificial neural network algorithms [36]. However, limited by the actual computational capacities, this emission model generally has to get accurate results at the cost of soaring time expenditure, which makes it not a practicable solution.

Due to numerous influence factors, vehicle emissions are often considered as comparatively complicated functions. However, to determine the amount of emissions at an acceptable time cost is of vital importance to the control algorithm design of EMS for the investigated P3 HEV powertrain, especially in the real-time online control scenario. As a consequence, an appropriate approximation method has to be employed to speed up the control algorithm for the sake of improving practicability. In this paper, a quadratic regression model is applied to indicate the emission performance for both computing time and conformance requirements reasons. First, it is fairly easy to determine the optimum point of a quadratic function, which means the time expenditure can be affordable. Second, the mathematical expressions of emission estimation model are supposed to be in consistency with previously established calculation models for energy consumption. In Section 2.2, quadratic polynomial fitting is adopted to determine the specific consumed power of both chemical energy and electric energy. Similar to Equation (1), the emission rate prediction equation is shown as follows:

$$ER = p_{1,i} + p_{2,i} M_{ICE} + p_{3,i} M_{ICE}^2 \tag{8}$$

where i refers to specific emissions (NOx or particle), $p_{1,i}$, $p_{2,i}$, and $p_{3,i}$ are fitting coefficients. In accordance with Equation (1), Equation (8) holds on the basis of constant engine speed n, which means the specific values of fittings coefficients $p_{1,i}$, $p_{2,i}$, and $p_{3,i}$ will change along with engine speed. In order to obtain the detailed coefficient configurations of Equation (8) under all operation conditions, massive efforts have been contributed to corresponding emission testing of the ICE in the investigated P3 HEV powertrain. As mentioned above, NOx and particle are determined as two main considerations for emission performance evaluation. Foundational emissions map of these pollutants are plotted based on the experimental data as shown in Figure 4. It should be noted that the amount of NOx is measured in grams per kilowatt hour while that of particle is represented by the detected specific blackening values (SBV, a unitless quantitative evaluation index employed to reflect the amount of particle in exhaust gas) per kilowatt hour. Additionally, what needs to be emphasized is that currently HEVs equipped with catalytic converters would almost completely clean out the NOx emissions under proper operating temperatures, so that the NOx optimization results after applying the proposed control algorithm would be non-significant if the NOx emission data acquisition was performed after the catalytic converter. Consequently, we collect the emission data directly from the exhaust pipe located before the catalytic converter when carrying out corresponding bench test. First, the measured numerical values of NOx emissions cease to be negligible, which subsequently highlights the contrast effect before and after optimization. Secondly, this experimental operation has little impact upon the measured values of the other pollutant particle. Considering that the following proposed control algorithm mainly targets at the realization of particle emissions reduction, this simplified operation not totally conforming to the real NOx emissions scenario is considered tolerable.

The family of relation curves between specific emission rate and engine torque are plotted in Figure 5. Similar to Figures 2 and 3, experimental data are marked as cross dots with different colors indicating different engine speed. Comparing the measured experimental data with related quadratic polynomial fitting curves, we can reach a conclusion that the fitting results show good agreement with the raw data. In particular, the variation tendency of original particle data points is comparatively complicated as shown in Figure 5b. Apparently, a simple quadratic function is not accurate enough to fit the data. In order to make the fitting curve match the original data points better, a piecewise quadratic function is brought into the fitting process. In addition, the demarcation point is self-adjusting under different engine speed circumstances to reach precise fitting results.

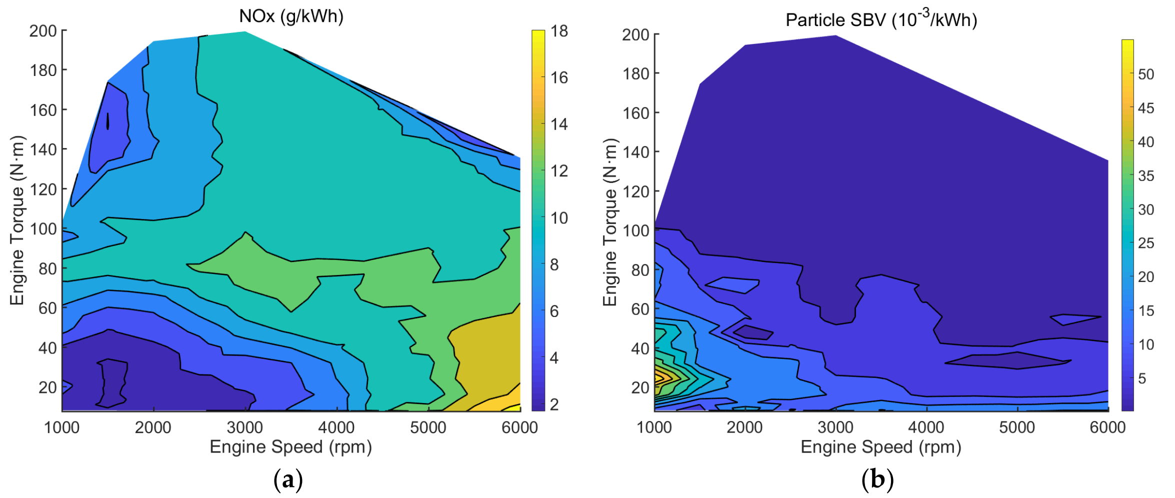

Figure 4. Emissions map of two main pollutants: (**a**) NOx and (**b**) Particle.

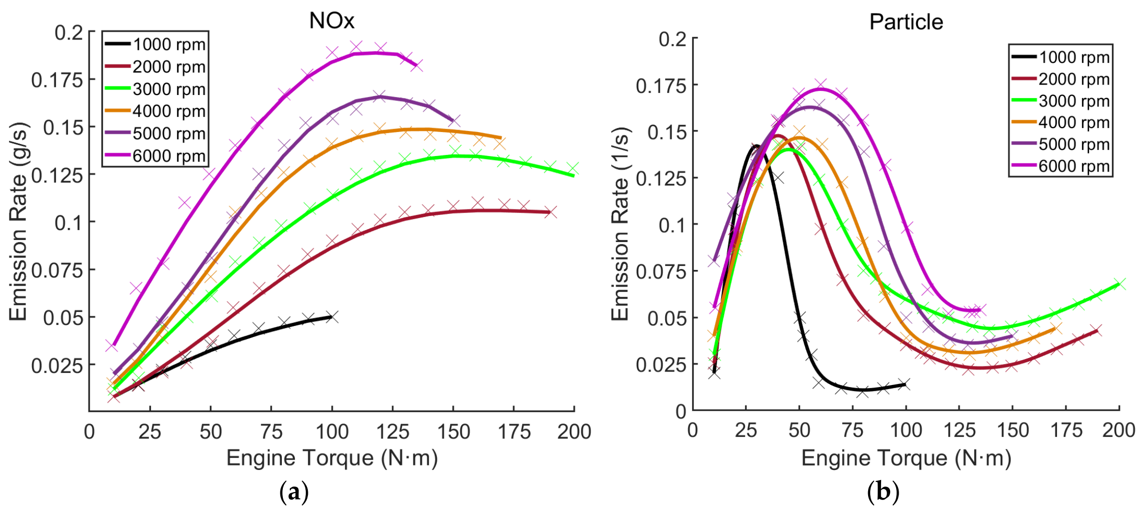

Figure 5. Quadratic polynomial fitting results of two main pollutants: (**a**) NOx and (**b**) Particle.

In general, the indicators of both energy consumption and emission performance are modeled by means of quadratic polynomial fitting method, which lays a solid foundation for subsequent control algorithm design. Based on the existing fitting results, the consumed power and specific emission rate can be incorporated into an integral objective function because of their parallel structures of mathematical expressions.

3. Control Algorithm Design for EMS

3.1. Combined Objective Function Establishment

In order to simultaneously account for the indicators of energy consumption and emission performance, appropriate multi-objective optimization method should be employed. For the control algorithm of EMS for HEVs, DP, and ECMS are commonly used methods [37]. The former adopts a traverse approach to get the global optimum solution, while the latter usually establishes a comprehensive fuel consumption cost function by means of making the instantaneous consumed battery energy equivalent to fuel consumption of the ICE:

$$\dot{m}_{eqv} = \dot{m}_f + \dot{m}_{batt,eqv} = \dot{m}_f + \alpha_{ef} \cdot \frac{E_{batt}}{LHV} \cdot \dot{\text{SOC}} \tag{9}$$

where $\dot{m}_{eqv}$ is overall equivalent fuel consumption rate, $\dot{m}_f$ is the actual fuel consumption rate of ICE, $\dot{m}_{batt,eqv}$ is the equivalent fuel consumption rate of consumed battery energy, α_{ef} is an equivalence factor applied to convert consumed battery energy into fuel consumption rate, E_{batt} is consumed battery energy, LHV is the low heating value of used fuel, and $\dot{\text{SOC}}$ is the derivative of the state of charge. Compared with DP, which needs the specific configurations of complete driving cycle, EMCS shows unique advantages in undemanding applications and fast algorithm speed, which consequently makes the online implementation a practicable reality under precise parameter calibration [38]. In this paper, a multi-parameter objective function is established on the grounds of ECMS as follows:

$$J_{MP}(t) = P_e(M_{ICE}, n) + \lambda \cdot P_m(M_{MOT}, n) + \mu \cdot ER(M_{ICE}, n) \tag{10}$$

where $J_{MP}(t)$ is the calculation value of the multi-parameter objective function at any time step, $P_e(M_{ICE}, n)$ is the calculation value of the chemical energy consumed power, $P_m(M_{MOT}, n)$ is the calculation value of the electric energy consumed power, and $ER(M_{ICE}, n)$ is the calculation value of the emission rate of specific emissions (NOx or particle). Both $P_e(M_{ICE}, n)$ and $ER(M_{ICE}, n)$ are the function of engine torque M_{ICE} and engine speed n, while $P_m(M_{MOT}, n)$ is the function of motor torque M_{MOT} and engine speed n. $P_m(M_{MOT}, n)$ is less than the battery capacity decrease because of efficiency loss, whereas battery efficiency coefficient λ is adopted in order to describe the health status of vehicle battery. μ is the weighting coefficient of emission performance and the change of μ has a significant impact on the subsequent control strategy. Higher μ means that objective function pays more attention to emission performance, while lower μ indicates that consideration of energy consumption reduction is more preferred in the search process for optimal solution.

As shown in Figures 2, 3 and 5, numerical values of the three parameters $P_e(M_{ICE}, n)$, $P_m(M_{MOT}, n)$, and $ER(M_{ICE}, n)$ differ greatly. To eliminate the adverse effect caused by excessive numerical value differences, normalization is employed as a dimensionless method as shown in following equations:

$$\begin{cases} P_{en} = \frac{P_e(M_{ICE}, n)}{P_e(M_{ICE}, n)_{max}} \\ P_{mn} = \frac{P_m(M_{MOT}, n)}{P_m(M_{MOT}, n)_{max}} \\ ER_n = \frac{ER(M_{ICE}, n)}{ER(M_{ICE}, n)_{max}} \end{cases} \tag{11}$$

where P_{en}, P_{mn}, and ER_n are all non-dimensional parameters, $P_e(M_{ICE}, n)_{max}$,$P_m(M_{MOT}, n)_{max}$, and $ER(M_{ICE}, n)_{max}$ refer to corresponding maximum numerical values during all calculation time steps, respectively. Combined with previously obtained quadratic fitting results, each of these three key factors can be determined through followed equations:

$$\frac{P_e(M_{ICE}, n)}{P_e(M_{ICE}, n)_{max}} = \frac{p_{1,ICE} + p_{2,ICE} \cdot \frac{\frac{M_{dem}}{i_0} - M_{MOT} i_m}{i_g} + p_{3,ICE} \cdot \left(\frac{\frac{M_{dem}}{i_0} - M_{MOT} i_m}{i_g} \right)^2}{P_e(M_{ICE}, n)_{max}} \tag{12}$$

$$\frac{P_m(M_{MOT}, n)}{P_m(M_{MOT}, n)_{max}} = \frac{p_{1,MOT} + p_{2,MOT} M_{MOT} + p_{3,MOT} {M_{MOT}}^2}{P_m(M_{MOT}, n)_{max}} \tag{13}$$

$$\frac{ER(M_{ICE}, n)}{ER(M_{ICE}, n)_{max}} = \frac{p_{1,ER} + p_{2,ER} \cdot \frac{\frac{M_{dem}}{i_0} - M_{MOT} i_m}{i_g} + p_{3,ER} \cdot \left(\frac{\frac{M_{dem}}{i_0} - M_{MOT} i_m}{i_g} \right)^2}{ER(M_{ICE}, n)_{max}} \tag{14}$$

$$J_{MP}(t) = P_{en} + \lambda \cdot P_{mn} + \mu \cdot ER_n = \frac{P_e(M_{ICE}, n)}{P_e(M_{ICE}, n)_{max}} + \lambda \cdot \frac{P_m(M_{MOT}, n)}{P_m(M_{MOT}, n)_{max}} + \mu \cdot \frac{ER(M_{ICE}, n)}{ER(M_{ICE}, n)_{max}} \quad (15)$$

where $p_{1,ICE}, p_{2,ICE}, p_{3,ICE}, p_{1,MOT}, p_{2,MOT}, p_{3,MOT}, p_{1,ER}, p_{2,ER}, p_{3,ER}$ are fitting coefficients, M_{dem} is the total demanded torque of the investigated P3 HEV. The original multi-parameter objective function in Equation (10) is updated as displayed in Equation (15). Above equations confirm that $J_{MP}(t)$ can be considered as a quadratic function of motor torque under all operation conditions. Earlier analysis has revealed that both $P_m(M_{MOT}, n)$ and $ER(M_{ICE}, n)$ are piecewise quadratic functions. The demarcation point of the former is always zero while that of the latter varies under different operation conditions, which means there are two demarcation points over full torque range. Considering that $J_{MP}(t)$ is the linear combination of these three crucial parameters, it is clear that $J_{MP}(t)$ is a piecewise quadratic function divided into three continuous intervals.

With regard to a three-stage piecewise quadratic function, a conclusion that can be drawn is that the optimal point must be selected from two boundary points, two demarcation points, and extreme points. As displayed in Figure 6, boundary points are marked with purple circles and demarcation points are marked with blue circles, while all existing extreme points are marked with green circles. For this scenario, the optimal point is marked with a red round dot. Planned comparisons lead to the conclusion that the identification of the optimal point can be performed accurately and promptly, which consequently guarantees the computation speed of subsequent control algorithm. As shown in Figure 6, M_{op} refers to the determined optimal motor torque within the range from M_{lb} to M_{ub} and $J_{MP}(t)_{min}$ is the corresponding minimum value of the multi-parameter objective function established in Equation (15).

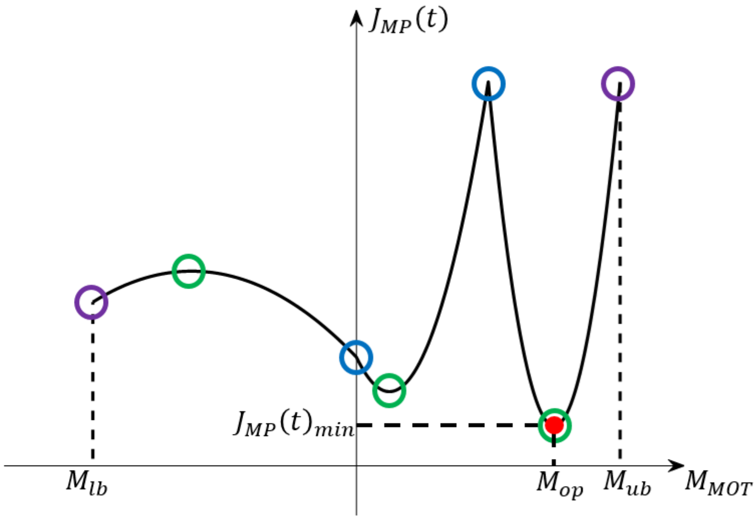

Figure 6. The optimal point identification for one scenario.

What calls for special attention is that the related part of the piecewise quadratic function can be regarded as a part of parabola going upward or downward in each interval. Considering that there are three intervals divided by two demarcation points (one demarcation point is zero while the other is indeterminate), 23 or 8 scenarios of the specific trend of the piecewise quadratic curve are supposed to be obtained. Furthermore, the indeterminate demarcation point may be positive or negative, which results in that all possible scenarios amounts to 8 × 2 = 16, as displayed in Figure 7. What needs illustration is that the identification process of the optimal point for each scenario of the 16 is nearly the same as demonstrated in Figure 6, thus there is no more detailed description.

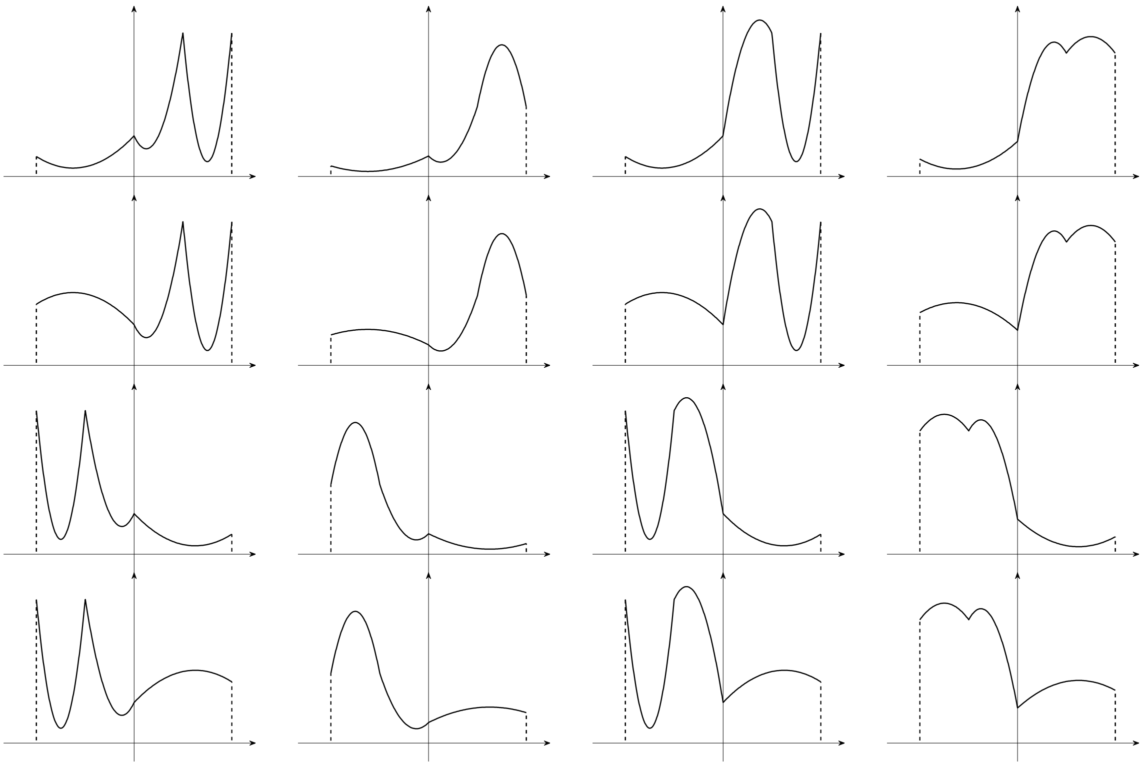

Figure 7. All possible scenarios of the piecewise quadratic function.

3.2. Algorithm Flow Design

Figure 8 shows a unified modeling language (UML) activity diagram for the proposed control algorithm. Considering that battery efficiency coefficient λ is generally unknown before the process of algorithm implementation, the initial iteration value λ_0 within the range from λ_{min} to λ_{max} is determined at the beginning. Moreover, the initial value of the state of charge SOC_0 and weighting coefficient μ are input as default parameters. Based on the related simulation model established in MATLAB/SIMULINK, M_{dem}, $J_{MP}(t)_{min}$, the optimal M_{MOT}, and corresponding M_{ICE} at each time step of the whole driving cycle are calculated sequentially.

With regard to the investigated P3 HEV, an obvious conclusion that can be drawn is that better driving experience comes from lower battery replacement frequency. In consideration of the non-rechargeable characteristic of the on-board power battery, its battery capacity is expected to maintain at the original level as much as possible with vehicle tested by a complete driving cycle, owing in large measure to appropriate control algorithm of EMS. Consequently, the proposed control strategy is performed around the premise that SOC_{final} of vehicle battery must equal to the original status after a complete driving cycle. A crucial constraint condition is set in search for the certain value of λ. The current SOC of vehicle battery is calculated at each time step and SOC_{final} will be determined after all time steps of the complete driving cycle have been calculated. Detailed configurations of the control algorithm for the complete driving cycle can be abstracted from previous calculation results on condition that SOC_0 equals to SOC_{final}; otherwise, the bisection method will be applied to iterate the specific value of λ and the preceding algorithm flow will be re-executed until the constraint condition has been satisfied. Another point to note is that the impact of weighting coefficient μ upon the final control algorithm results can be investigated by replacing the preset value of μ with another one at the start of algorithm flow, as displayed in Figure 8. In general, the inputs of the proposed control algorithm include the initial value of SOC (SOC_0), the initial iteration value of λ (λ_0), the range constraint for λ (upper bound λ_{max} and lower bound λ_{min}), the preset weighting coefficient of emission performance μ, the demanded vehicle velocity v, and vehicle acceleration a at each time step of the complete driving cycle (WLTP). Moreover, engine torque M_{ICE} and motor torque M_{MOT} are determined as the control input.

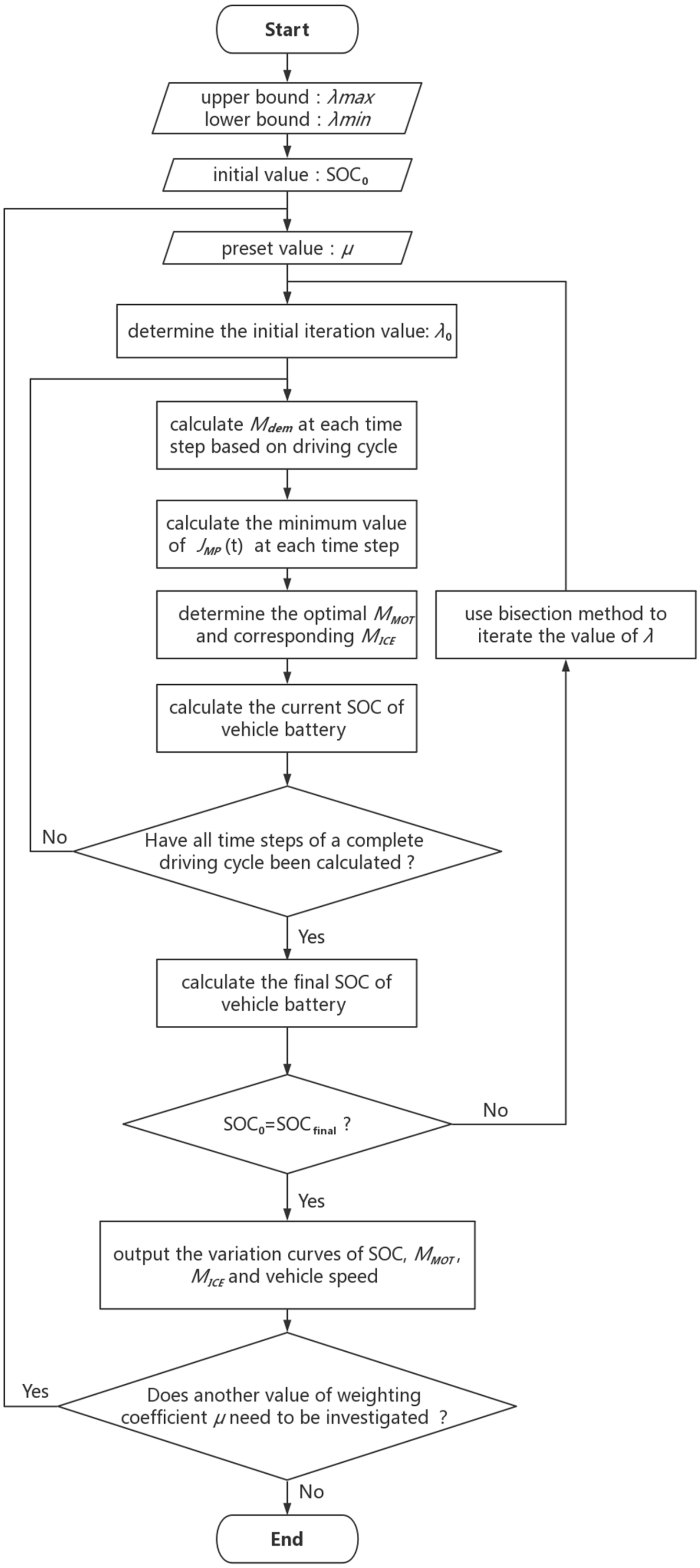

Figure 8. Unified modeling language (UML) activity diagram for the control algorithm.

As mentioned above, a corresponding simulation model is established in MATLAB/SIMULINK environment. With respect to the optimization solver, there are four general categories of solvers internally installed in the MATLAB/SIMULINK optimization toolbox: Minimizers, Multi-Objective minimizers, Equation solvers, and Least-Squares (curve-fitting) solvers. Among them the last one attempts to minimize a sum of squares. This type of problem frequently arises in fitting a model to data. As a consequence, this group of solvers is commonly used to address problems of finding nonnegative solutions, bounded or linearly constrained solutions, and fitting parametrized nonlinear or linear models to data. Coincidentally, the optimization problem targeted at $J_{MP}(t)$ fits into this category. Therefore, Least-Squares (curve-fitting) solvers are selected in consideration of their good compatibility with the proposed control algorithm.

4. Simulation Results Analysis

4.1. Driving Cycle Selection

The previously established control algorithm model should be tested against the actual urban driving conditions to prove its practicability. Considering that the investigated P3 HEV is oriented around the Europe and China auto market, mainstream driving cycles including the New European Driving Cycle (NEDC) and the aforementioned WLTP should be selected before further comparison.

Figure 9 displays the complete velocity profile of the NEDC. Both urban and suburban driving conditions are taken into consideration in NEDC to guarantee that the driving performance of vehicle can be accurately tested most of the time. However, it should be noted that NEDC is composed of different uniform-acceleration, uniform-speed, and uniform-deceleration processes, which makes it less approximate to the actual driving conditions as we all know that it is nearly possible for drivers to maintain at a constant speed or acceleration under the circumstance of actual road running. Past investigations have shown that NEDC is not representative for real-world vehicle usage because the emissions and fuel consumption of the vehicles are underestimated. With emissions regulations tightening continuously, NEDC has been replaced by WLTP in Europe since Sept. 1st 2018 due to its inadequacy in test precision [39,40].

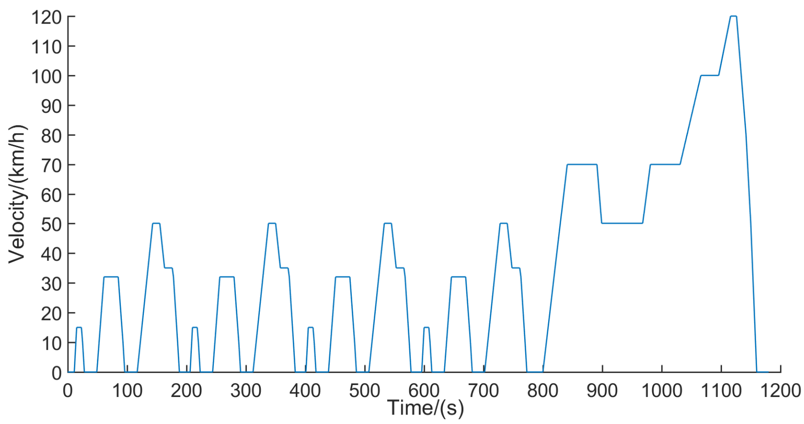

Figure 9. The velocity profile of the New European Driving Cycle (NEDC).

As shown in Figure 10, it is clear that the velocity profile of the WLTP is comparatively sophisticated, aiming at a more dynamic and worldwide harmonized test cycle. Considering that the WLTP is closer to real-world driving and has become the new type approval test in Europe, WLTP is ultimately selected as the driving cycle for simulation. Corresponding configurations are presented in Table 3 [41,42].

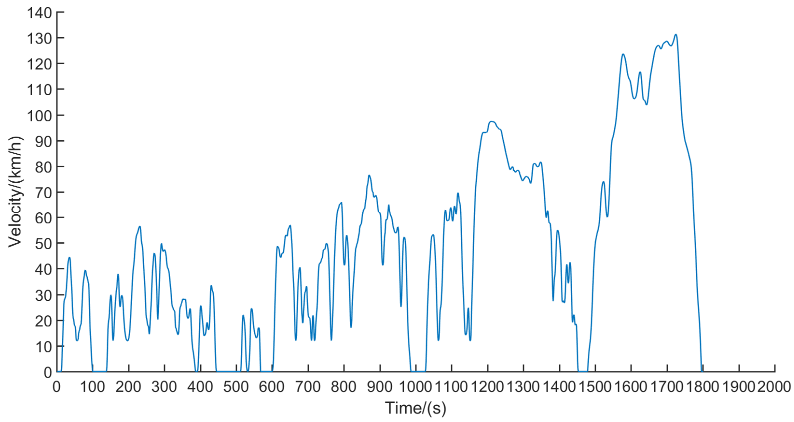

Figure 10. The velocity profile of the Worldwide-Harmonized Light-Vehicle Test Procedure (WLTP).

Table 3. WLTP velocity profile configurations.

Parameters	Value
Cycle distance	23.26 km
Cycle time	1800 s
Average velocity	46.52 km/h
Maximum velocity	131.3 km/h
Maximum acceleration	1.75 m/s^2
Maximum deceleration	−1.72 m/s^2

4.2. Simulation Results with Different Weighting Coefficients

It should be noted that all those fitting coefficients in Equations (12)–(15) play an important role in determining the specific value of $J_{MP}(t)$. However, considering the huge amount of fitting data (the whole operation conditions are supposed to be included) and space limitation, corresponding fitting coefficients table are not presented in this paper. Additionally, specific configurations of the investigated P3 HEV are listed in Table 4. It needs to be emphasized that a series of discrete values of μ is determined as algorithm input to further explore the impact of weighting coefficient upon the control strategy. μ_{max} is set as 0.2 while μ_{min} is set as 0. As mentioned above, the realization of particle emissions reduction is our primary concern in the present study. Therefore, these two most representative scenarios for particle are investigated in detail with simulation results shown as follows:

Table 4. P3 HEV configurations in simulation model.

Parameters	Value	Parameters	Value
i_0	4	m	1615 kg
i_g	4.6/3.3/2.3/1.7/1.29/1/0.84	f_r	0.01
R	353.1 mm	λ_{max}	10
i_m	3.5	λ_{min}	1
c_d	0.37	SOC_0	70%
A	1.88 m^2	λ_0	1.25
ρ_{air}	1.188 kg/m^3	μ	0~0.2

With respect to different weighting coefficients, the simulation results of μ_{min} are presented in Figure 11a,c, contrasted with those of μ_{max} in Figure 11b,d. As shown in Table 3, the cycle time of WLTP is 1800 s. It should be noted that the time step in the MATLAB/SIMULINK model is set as 1 s, which indicates that all operation condition points of the complete WLTP cycle amount to 1800. Red cross dots in Figure 11 represents these operating points.

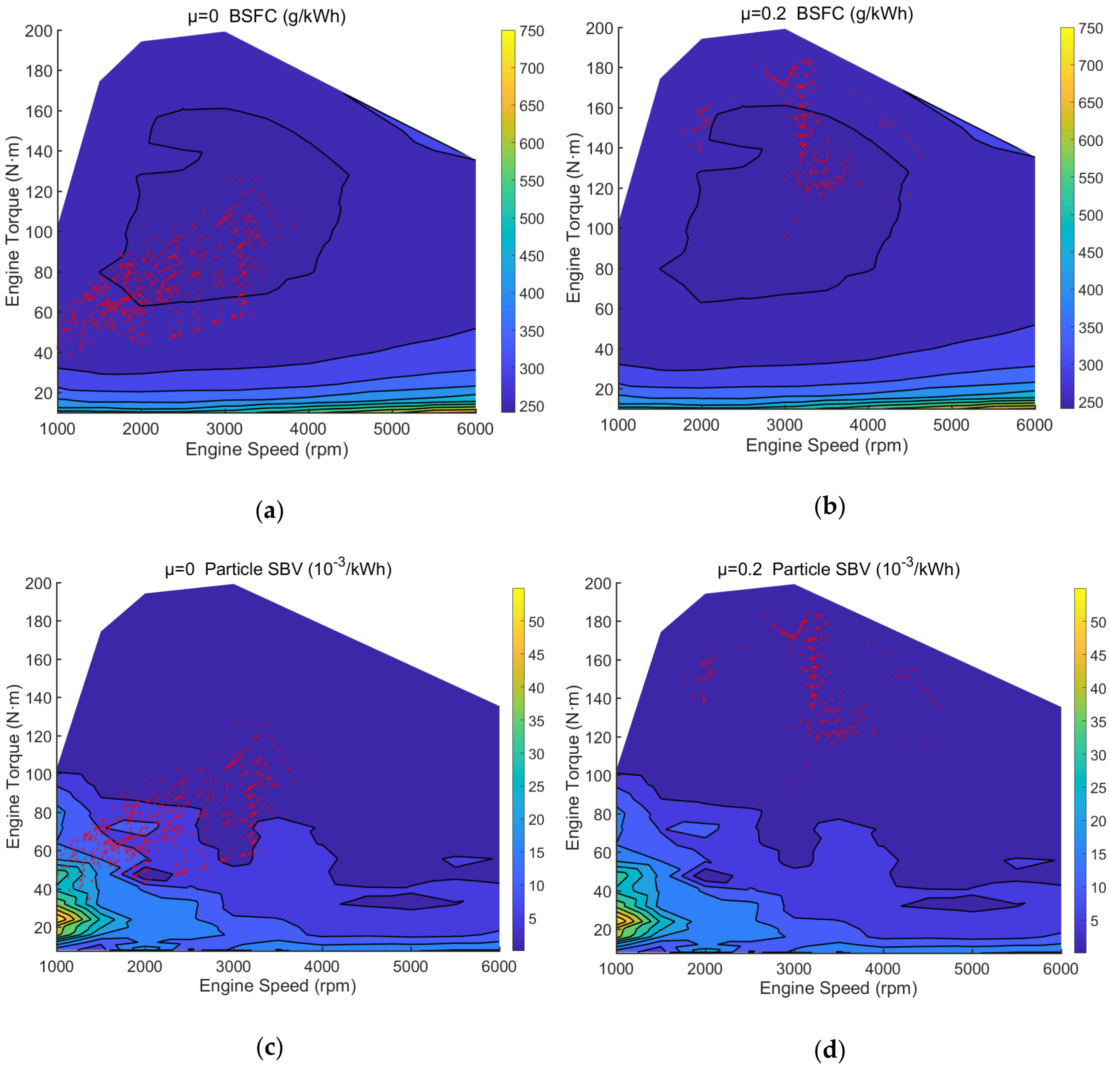

Figure 11. Comparison results of different weighting coefficients for emission particle. (**a**) $\mu = 0$ BSFC; (**b**) $\mu = 0.2$ BSFC; (**c**) $\mu = 0$ Particle SBV; (**d**) $\mu = 0.2$ Particle SBV.

Applying Equation (10), it is clear that the leverage of emission performance will be not taken into consideration in the μ_{min} scenario. Comparing Figure 11a,b, it can be concluded that the distribution status of brake specific fuel consumption (BSFC) values of all operating points fails to change significantly with μ increasing from 0 to 0.2. In the μ_{min} scenario where the established objective function only pays attention to energy consumption, nearly half of all operating points are located in the optimal fuel economy area while the other half are mainly located at its periphery area as shown in Figure 11a. By contrast, the above situation seems to stay the same in the μ_{max} scenario where emission performance influence plays an important role as exhibited in Figure 11b, which implies that the overall fuel consumption of these two scenarios are roughly equivalent.

Nevertheless, remarkable differences can be observed when it comes to the amount of particle represented by specific blackening values between these two scenarios. As shown in Figure 11d, operating points are more concentrated in the low SBV area with emission performance assigned with a higher weight in the process of constructing objective function in Equation (10). Comparatively, the distribution status of the μ_{min} scenario appears not as good as the other one. As shown in Figure 11c, quite a few operating points situate in the high SBV area, which means more particle emissions during the whole WLTP test cycle.

Figures 12 and 13 show the variation curves of crucial state parameters including SOC, engine torque, motor torque, and gear of μ_{min} and μ_{max} scenarios, respectively. Associated with the velocity profile of WLTP presented in Figure 10, comparative analysis leads to the conclusion that the engine generally runs in the relatively high-torque region in the μ_{max} scenario. Simultaneously, the frequency of recharging and discharging of the vehicle battery, which is represented by the degree of fluctuation observed in the SOC or motor torque variation curves, is slightly higher. Conversely, the frequency of the gear shift is strikingly lower than that of the μ_{min} scenario; the corresponding control algorithm will provide the driver with a relatively simple gear shift strategy during the whole WLTP test cycle under the circumstance of the preset value μ_{max}. Obviously, relevant adjustment of gear shift strategy makes contribution to the driving experience improvements for the driver.

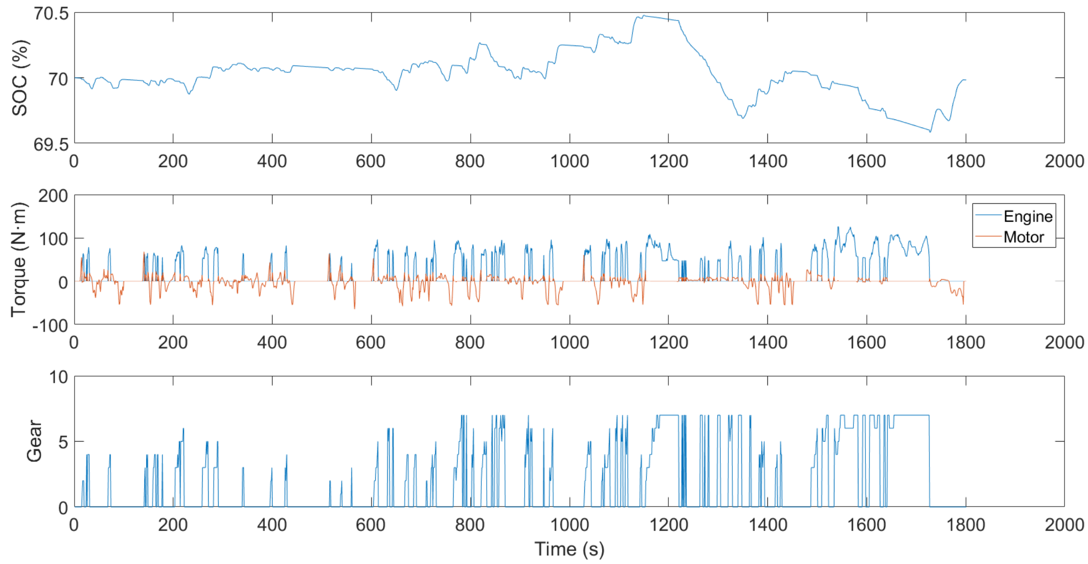

Figure 12. Three state parameters' variation curves of μ_{min} for emission particle.

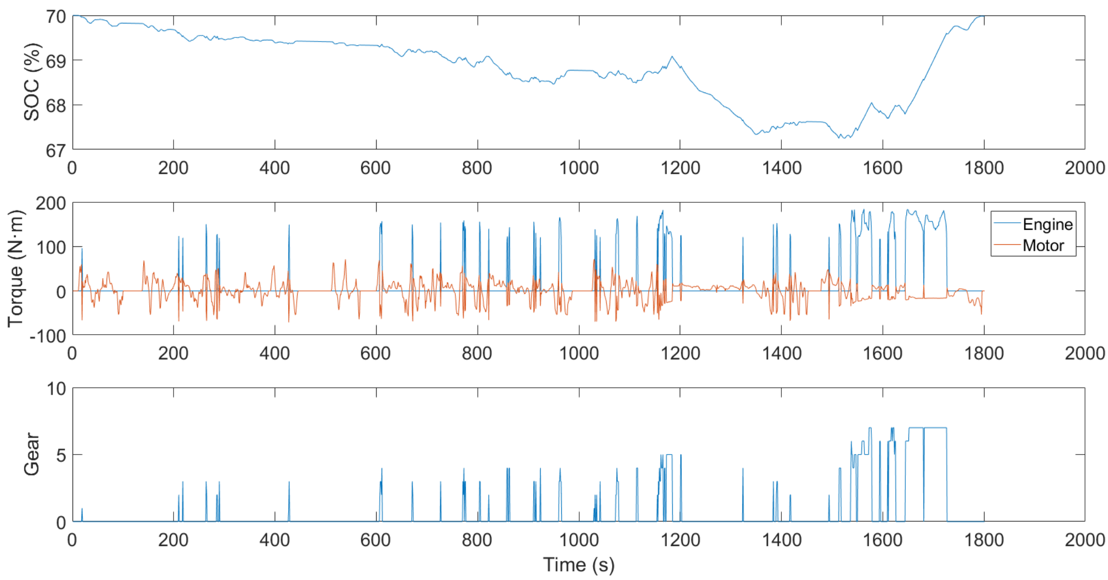

Figure 13. Three state parameters' variation curves of μ_{max} for emission particle.

Figure 14 displays the variation curves of SOC during the whole WLTP test cycle pertaining to different μ for emission particles. It can be observed that the maximum decreasing amplitude of SOC grows larger with μ gradually increasing. Considering that the higher μ is, the more attention will be paid to the optimization of emission indicators. As a consequence, the operation range of engine is supposed to be obliged to "comparatively low emissions area" (i.e., the darker areas in Figure 4b) in pursuit of the fulfillment of emission performance considerations. Comparison results in Figure 14 provide solid evidence that motor will make greater contribution to overall power output to compensate the underpowered engine. It is in perfect accordance with the relevant facts demonstrated by the motor variation curves shown in Figures 12 and 13 that motor will act more as a role of power output instead of power generation under the higher μ circumstance. Meanwhile, it is confirmed again that the preset constraint condition SOC_0 must equal SOC_{final} and further, that is strictly satisfied under different μ circumstances.

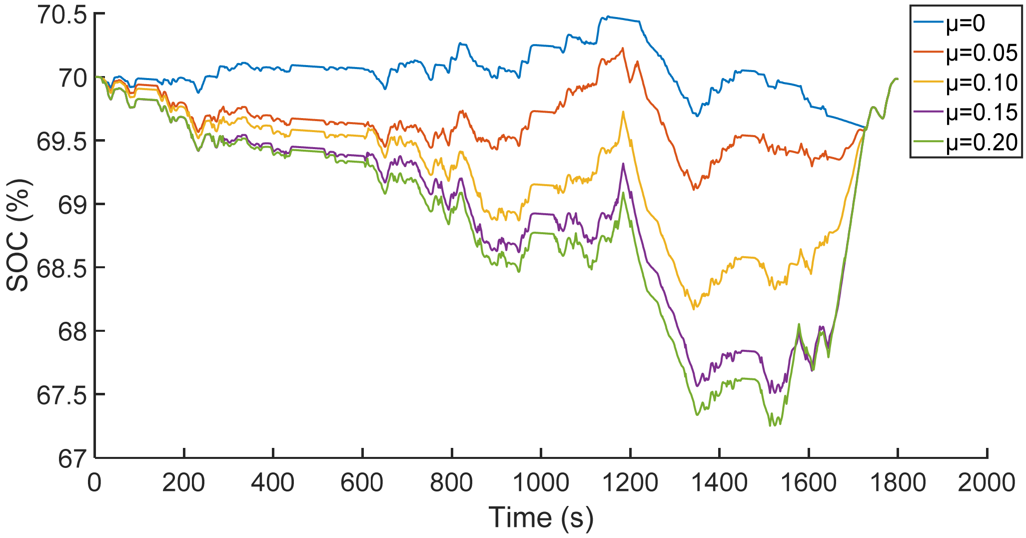

Figure 14. The variation curves of SOC pertaining to different μ for emission particle.

In terms of corresponding simulation results for the other pollutant NOx, similar conclusions can be reached through the same analysis. Due to space limitation, detailed result figures of NOx are presented in Appendix A.

Combining all the simulation results of the series of discrete values μ for both particle and NOx, Figure 15 exhibits the relationship between emission performance and fuel consumption (FC) based on the 20 obtained sets of data; specific values are listed in Table A1 in Appendix A. The data points of particle are marked as 20 red plus dots; those of NOx are marked as blue cross dots. Considering the complete WLTP test cycle, the calculation results of each time step add up to the integrated FC in L/100km and total emissions (i.e., NOx emissions in grams and particle emissions in SBV). As shown in Figure 15, data points located from top left to bottom right signify the simulation results of increasing μ for both exhaust pollutants. By analysis of the curve trend, it is clear that there exists a trade-off relationship between fuel economy and emission performance, whether it is for NOx or particle. As the weighting coefficient μ grows up, relevant results indicating worse fuel economy and better emission performance simultaneously are attained through simulation, which also conforms to a previous inference derived from $J_{MP}(t)$, set up in Equation (15).

Considering that the investigated P3 HEV is oriented at Europe and China auto market, both the latest European emission standard (i.e., Euro 6c) and the Chinese counterpart (i.e., China VI) are investigated and the emission limits of particle and NOx are shown in Table 5 [43–47]. Moreover, the simulation results obtained from the two most representative scenarios (i.e., $\mu_{min} = 0.00$ and $\mu_{max} = 0.20$) are also presented in Table 5 as a contrast. It should be noted that the unit of particle emissions used in China VI and Euro 6c is the number (Nb) of particle per kilometer rather than SBV employed in this paper. Therefore, the conversion of the relevant numerical values is supposed to be performed beforehand. In terms of particle emissions, it can be concluded that the particle number (PN) is more than five times the limit of China VI/Euro 6c in the μ_{min} scenario where the established objective function only pays attention to energy consumption. Conversely, the PN succeeds in meeting the requirements of these two emission legislations in the μ_{max} scenario where the emission performance indicator is endowed with a substantial weight. An obvious conclusion that can be drawn is that the effectiveness of the proposed control algorithm is validated once again. With respect to NOx emissions, it is clear that μ_{min} or μ_{max} scenario yields results that significantly exceed the limits of the China VI/Euro 6c. As mentioned above, the experimental data of NOx emission is directly captured from the exhaust pipe located before the catalytic converter, which causes its numerical values considerable, thus the optimization effect will be heightened. Actually, HEVs are supposed to be equipped with catalytic converters in order to fulfil the relevant NOx limitations of the China VI/Euro 6c in the real world.

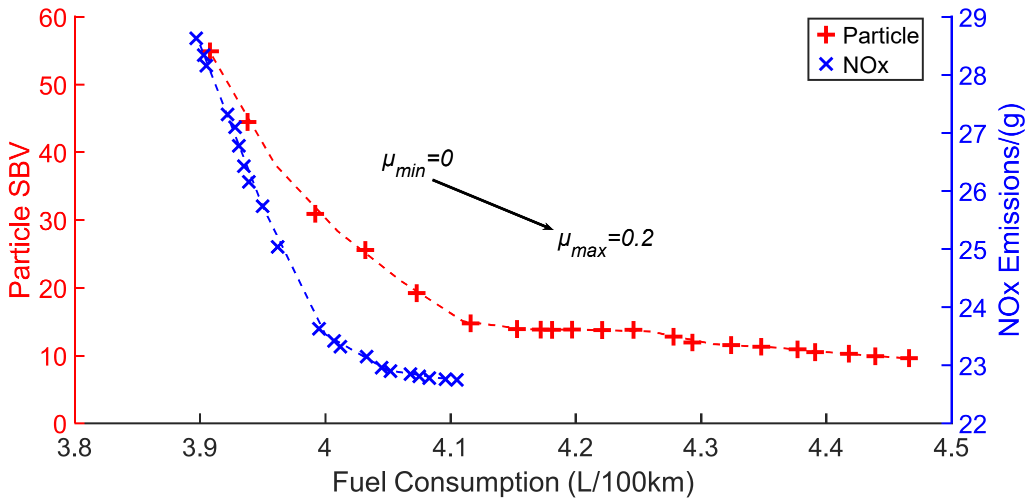

Figure 15. The combination of simulation results of the series of discrete values μ.

Table 5. Comparison between simulation results and the latest emission standards.

Scenarios	Particle Emissions (Nb/km)	NOx Emissions (mg/km)
$\mu_{min} = 0.00$	3.0×10^{12}	1231
$\mu_{max} = 0.20$	5.0×10^{11}	978
China VI	6.0×10^{11}	60
Euro 6c	6.0×10^{11}	75

4.3. Comparison between DP and ECMS

Actual execution time features prominently in the practicability of proposed algorithm. In the real world, classical DP algorithm is subject to online application restrictions in most cases because of prohibitive time expenditure. Nevertheless, a real sense of global optimal solution can be obtained by DP algorithm. In contrast to DP, solutions found by ECMS or other simplification algorithm generally suffer, to some extent, local optimal traps. Consequently, offline calculation results based on DP are commonly set as a reference for comparison [48–50].

As mentioned above, the proposed control algorithm design is developed on the basis of ECMS. Instead of applying quadratic polynomial fitting method for the sake of the simplification of objective function, the classical DP algorithm employs a comparatively straightforward traversal method in order to identify the specific location of the optimal point. During the optimization process of searching the minimal value of $J_{MP}(t)$, the DP algorithm basically calculates the specific values of $J_{MP}(t)$ under all possible operation conditions and sorts out the corresponding output torque configurations (i.e., M_{op}) for $J_{MP}(t)_{min}$. It should be noted that the detailed numerical calculation in the DP algorithm is predicated on the raw experimental data (e.g., the emissions map of two main pollutants particle and NOx as shown in Figure 4) rather than fitting results, which on the one hand guarantees the precision of the global optimal solution obtained by DP algorithm, but on the other hand makes it significantly time-consuming.

Considering both exhaust pollutants, Figure 16 displays the comparison between simulation results of DP and ECMS; the specific relative error (RE) data are presented in Table A2 in Appendix A. It can be concluded from Figure 16 that DP yields global optimal data points distinguishing from those local optimal counterparts of ECMS with only slightly perceptible difference, which thus demonstrates the accuracy and feasibility of the proposed control algorithm predicated on ECMS.

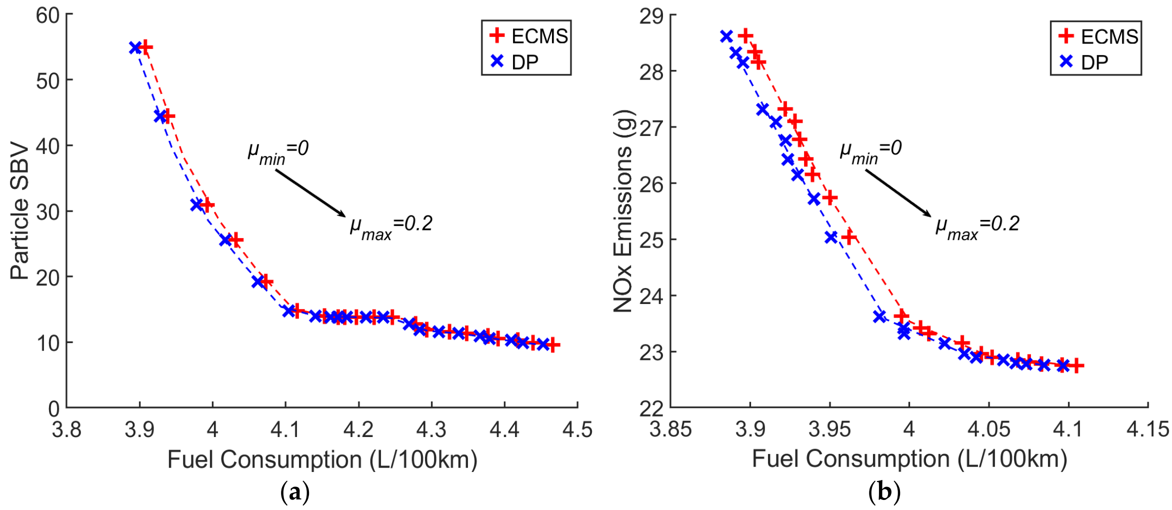

Figure 16. The comparison between simulation results of Dynamic Programming (DP) and Equivalent Consumption Minimization Strategy (ECMS): (**a**) Particle and (**b**) NOx.

5. Discussions and Conclusions

Continuous deterioration of the global atmospheric environment has given rise to the prosperity of so-called green vehicles. Therefore, HEVs have drawn extensive attention from academia and the automobile industry alike as a practicable technical route. With respect to the EMS design, which undoubtedly occupies an indispensable position in HEVs advance, strategic planning are in particular required in order to boost the overall performance improvement of the HEV powertrain. In consideration of tightening regulations on vehicle exhausts, it seems natural that there needs to be more concern about vehicle emission performance during the design process of the control algorithm design for the EMS in HEV powertrain.

However, few previous studies have deeply investigated a feasible control algorithm, simultaneously considering both energy consumption and emission performance. To illuminate the uncharted area, we present a novel design scheme incorporating the aforementioned two performance evaluation indicators into a single objective function based on ECMS. Massive bench test data have been collected as the prerequisite for subsequent modeling. Quadratic polynomial fitting method is appropriately applied into the process of determining the specific values of corresponding indicators. This operation not only guarantees that both consumed power and specific emission rate can be incorporated into an integral objective function because of their parallel structures of mathematical expressions, but it also significantly improves the computation speed of the proposed control algorithm because the identification process of the optimal point can be performed accurately and promptly.

Subsequently, a comprehensive multi-parameter objective function is established on the grounds of ECMS with the relevant simulation models constructed in MATLAB/SIMULINK. The proposed control algorithm design is validated against the simulation results predicated on WLTP. The impacts of weighting coefficients pertaining to two exhaust pollutants upon the specific configurations of the proposed control algorithm are discussed in detail. Furthermore, comparative analysis of the simulation results obtained from ECMS and classical DP algorithm, respectively, is performed. In the present study, we mainly focus on the algorithm structure design and preliminary simulation verification. Further, we think that the present research findings may not be optimal but should be sufficient to provide requisite guidance necessary for the appropriate design of control algorithm for EMS, which undoubtedly plays a vital role in the HEV powertrain performance improvement. Although demonstrated by preliminary simulation results, this proposed control algorithm design suffers from some limitations due to the lack of real road running experimental data from the vehicle equipped with the redesigned EMS. However, the obtained results can still cast a new light on the control algorithm design for EMS in HEV powertrain despite that inadequacy. Detailed analysis leads to the following conclusions:

1. The indicators of both energy consumption and emission performance are accurately modeled by applying the quadratic polynomial fitting method. Fitting results of corresponding relation curves show good agreement with the raw data obtained from bench test, which lays a solid foundation for subsequently incorporating the aforementioned considerations into the integrated objective function.
2. With respect to the related mathematical expression of the combined objective function, a three-stage piecewise quadratic function is attained. Furthermore, it is confirmed that the identification of corresponding optimal point can be performed precisely and promptly, which consequently yields significant computation speed advantages when compared with the classical DP algorithm.
3. Remarkable changes can be observed in the simulation results between weighting coefficients μ. Under the circumstance of emission performance assigned with a higher weight, findings prove that the operation range of engine is obliged to "comparatively low emissions area" while motor makes greater contribution to the overall power output. Considering the series of discrete values μ, analysis of curve trend demonstrates that there exists a trade-off relationship between fuel economy and emission performance, whether it is for NOx or particle.
4. A comparative investigation of the simulation results from ECMS and DP respectively validates the feasibility and accuracy of the proposed control algorithm design predicated on ECMS.

Author Contributions: Conceptualization, Y.S. and Y.Q.; Methodology, K.H.; Software, Y.S.; Formal Analysis, Y.Q.; Data Curation, Y.Q. and Y.S.; Writing-Original Draft Preparation, Y.Q.; Writing-Review and Editing, K.H. and Y.Q.

Funding: This research was funded by Beijing Municipal Science & Technology Commission grant number D17111000490000.

Acknowledgments: The authors gratefully acknowledge the administrative and technical support from Xiaonan Zhang M.Sc. and Markus Eisenbarth M.Sc. of RWTH Aachen University.

Conflicts of Interest: The authors declare no conflict of interest.

Nomenclatures

Abbreviations

HEVs	hybrid electric vehicles
PHEVs	plug-in hybrid electric vehicles
BEVs	battery electric vehicles
FCEVs	fuel cell electric vehicles
EMS	energy management system
V2I	vehicle to infrastructure
V2V	vehicle to vehicle
SGC	supervisory control system
MPC	Model Predictive Control
CS	charge sustaining

PMS	power management strategy
SMPCL	stochastic model predictive control with learning
ECMS	Equivalent Consumption Minimization Strategy
WLTP	Worldwide-harmonized Light-vehicle Test Procedure
DP	Dynamic Programming
HV	high voltage
ICE	internal combustion engine
A/F	air/fuel ratio
CO	carbon monoxide
HC	hydrocarbon
FTP	Federal Test Procedure
MEC01	1^{st} Version of the Modal Emissions
SBV	specific blackening value
UML	unified modeling language
BSFC	brake specific fuel consumption
FC	fuel consumption
Nb	Number
PN	particle number
RE	relative error
Symbols	
P_{EC}	chemical/electric energy consumed power
M_{EC}	corresponding output torque (engine torque/motor torque)
$p_{1,EC}, p_{2,EC}, p_{3,EC}$	fitting coefficients in Equation (1)
ER	specific emission rate
FR	fuel consumption rate
$g_{emissions}$	the mass of engine-out emissions
g_{fuel}	the mass of consumed fuel
CPF	catalyst pass fraction
C_0	weight coefficient in Equation (3)
ϕ	fuel/air equivalence ratio
C_1	emission index coefficient in Equation (3)
Γ	maximum catalyst CO/HC efficiency
C_F	stoichiometric *CPF* coefficient based on FTP Bag 2 cycle
C_M	enrichment *CPF* coefficient based on MEC01 cycle
$a_1, a_2, a_3, b_1, b_2, b_3, c_1, c_2, c_3$	regression coefficients in Equation (5)
v	vehicle velocity
a	vehicle acceleration
n	engine speed
i_0	the reduction gear ratio of main decelerator
i_g	the transmission ratio of gearbox
R	the radius of wheel
M_{ICE}	engine torque
M_{MOT}	motor torque
i_m	the transmission ratio of motor gearbox
c_d	aerodynamic drag coefficient
A	cross-sectional area
ρ_{air}	the mass density of ambient air
m	entire vehicle weight
f_r	rolling resistance coefficient
i	subscript indicating specific emissions (NOx or particle)
$p_{1,i}, p_{2,i}, p_{3,i}$	fitting coefficients in Equation (8)
$\dot{m}_{eqv}$	overall equivalent fuel consumption rate
$\dot{m}_f$	the actual fuel consumption rate of ICE

$\dot{m}_{batt,eqv}$	the equivalent fuel consumption rate of consumed battery energy
α_{ef}	equivalence factor
E_{batt}	consumed battery energy
LHV	the low heating value of used fuel
$\dot{\mathrm{SOC}}$	the derivative of the state of charge
$J_{MP}(t)$	the calculation value of the multi-parameter objective function at any time step
$P_e(M_{ICE}, n)$	the calculation value of the chemical energy consumed power
$P_m(M_{MOT}, n)$	the calculation value of the electric energy consumed power
$ER(M_{ICE}, n)$	the calculation value of the emission rate of specific emissions (NOx or particle)
λ	battery efficiency coefficient
μ	the weighting coefficient of emission performance
P_{en}	non-dimensional parameter for $P_e(M_{ICE}, n)$
P_{mn}	non-dimensional parameter for $P_m(M_{MOT}, n)$
ER_n	non-dimensional parameter for $ER(M_{ICE}, n)$
$P_e(M_{ICE}, n)_{max}$	the maximum value of $P_e(M_{ICE}, n)$ during all time steps
$P_m(M_{MOT}, n)_{max}$	the maximum value of $P_m(M_{MOT}, n)$ during all time steps
$ER(M_{ICE}, n)_{max}$	the maximum value of $ER(M_{ICE}, n)$ during all time steps
M_{dem}	the total demanded torque of the investigated P3 HEV
M_{op}	the determined optimal motor torque in Figure 8
M_{lb}	the lower bound of motor torque
M_{ub}	the upper bound of motor torque
$J_{MP}(t)_{min}$	the corresponding minimum value of $J_{MP}(t)$ in Figure 8
λ_{max}	the upper bound of λ
λ_{min}	the lower bound of λ
SOC_0	the initial value of the state of charge
λ_0	the initial iteration value of λ
SOC	state of charge
$\mathrm{SOC}_{\mathrm{final}}$	the final calculation value of the state of charge
μ_{max}	the maximum value of μ
μ_{min}	the minimum value of μ

Appendix A

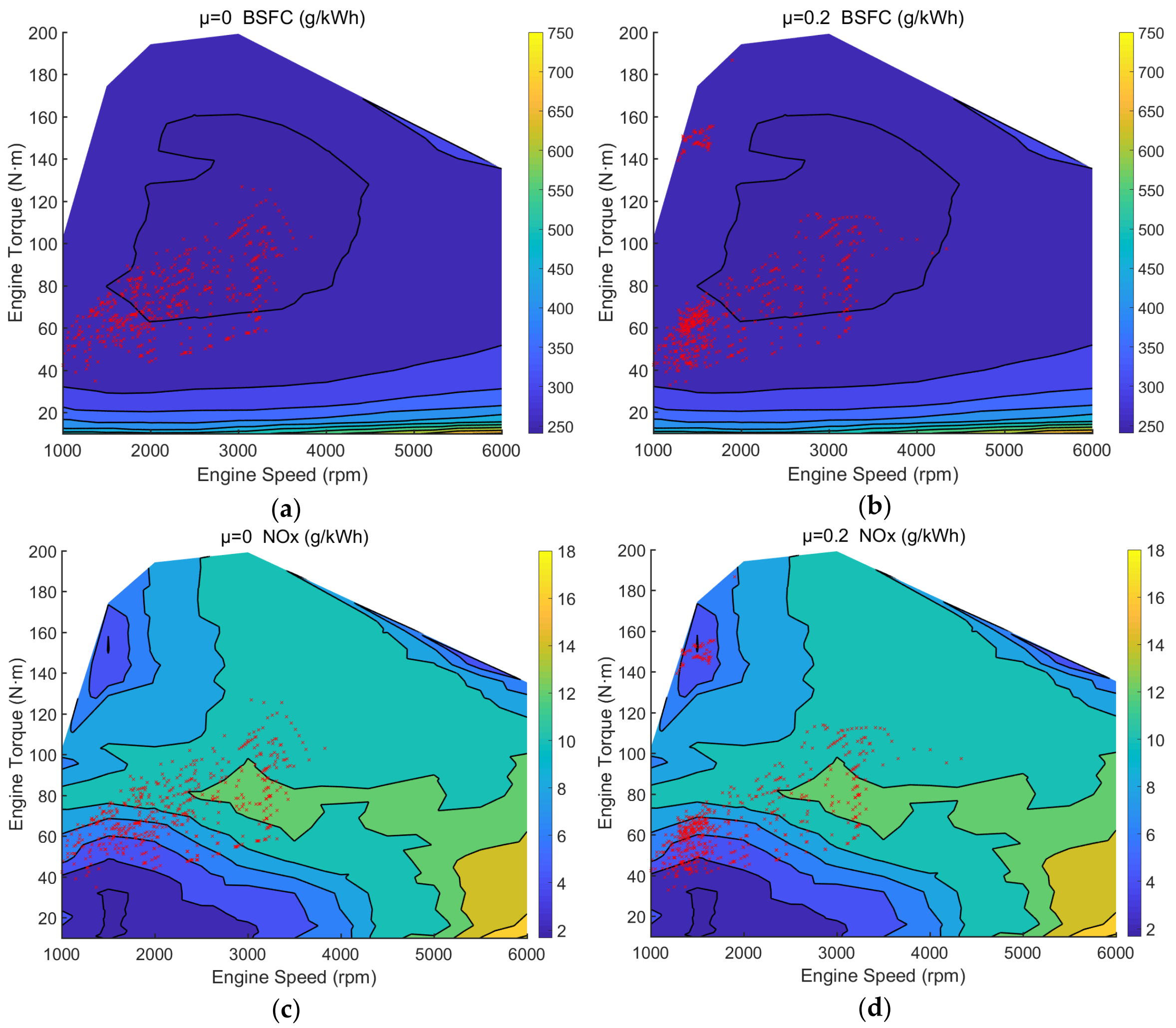

Figure A1. Comparison results of different weighting coefficients for emission NOx. (**a**) $\mu = 0$ BSFC; (**b**) $\mu = 0.2$ BSFC; (**c**) $\mu = 0$ NOx; (**d**) $\mu = 0.2$ NOx.

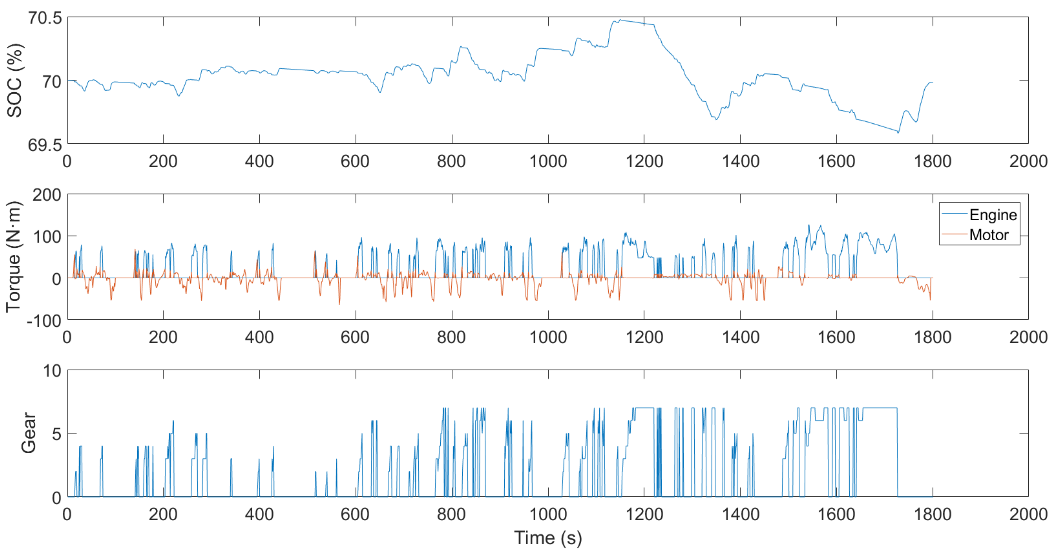

Figure A2. Three state parameters' variation curves of μ_{min} for emission NOx.

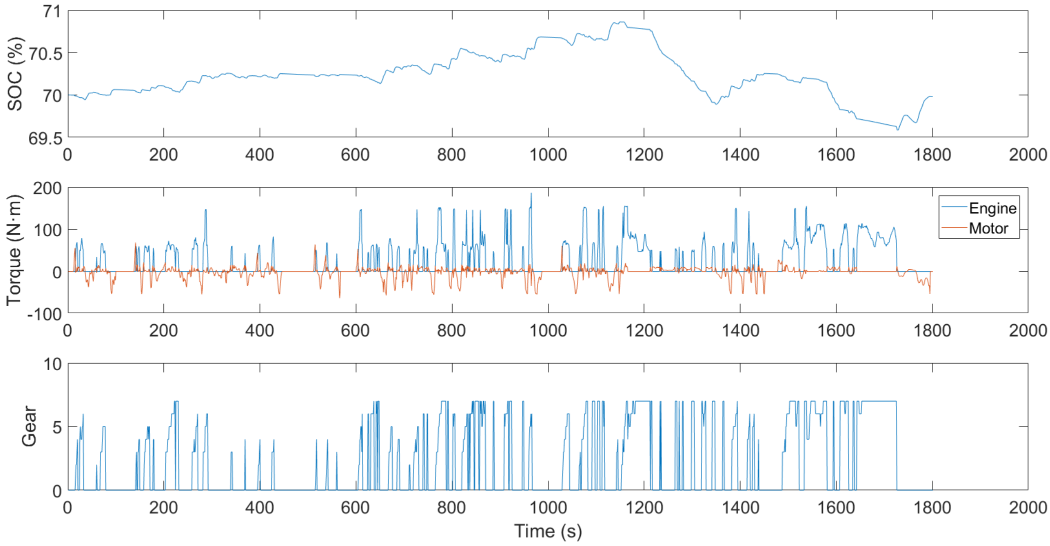

Figure A3. Three state parameters' variation curves of μ_{max} for emission NOx.

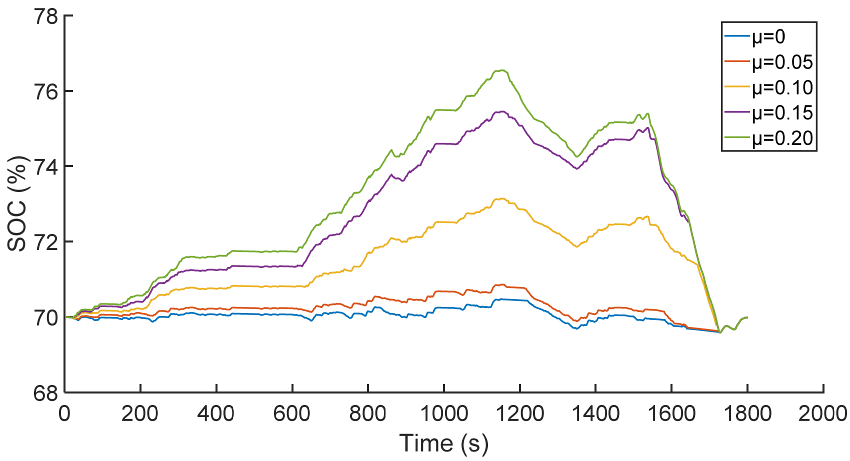

Figure A4. The variation curves of SOC pertaining to different μ for emission particle.

Table A1. The combination of simulation results of the series of discrete values μ.

μ	Particle		NOx	
	FC (L/100km)	**SBV(-)**	**FC (L/100km)**	**Emissions (g)**
0.00	3.908	54.92	3.897	28.63
0.01	3.938	44.48	3.903	28.34
0.02	3.992	30.94	3.905	28.16
0.03	4.032	25.57	3.922	27.32
0.04	4.073	19.21	3.928	27.10
0.05	4.116	14.76	3.931	26.78
0.06	4.153	13.93	3.935	26.43
0.07	4.172	13.84	3.939	26.16
0.08	4.181	13.82	3.950	25.74
0.09	4.197	13.84	3.962	25.04
0.10	4.221	13.79	3.995	23.63
0.11	4.246	13.82	4.007	23.42
0.12	4.278	12.80	4.012	23.32
0.13	4.293	11.93	4.033	23.15

Table A1. *Cont.*

μ	Particle		NOx	
	FC (L/100km)	**SBV(-)**	**FC (L/100km)**	**Emissions (g)**
0.14	4.324	11.56	4.045	22.96
0.15	4.348	11.32	4.052	22.90
0.16	4.377	10.92	4.068	22.85
0.17	4.391	10.51	4.075	22.81
0.18	4.418	10.29	4.083	22.78
0.19	4.439	9.90	4.096	22.76
0.20	4.466	9.63	4.105	22.75

Table A2. The relative error between simulation results of DP and ECMS.

μ	Particle		NOx	
	FC RE (%)	**SBV RE (%)**	**FC RE (%)**	**Emissions RE (%)**
0.00	0.252	0.019	0.256	0.045
0.01	0.217	0.031	0.334	0.036
0.02	0.206	0.089	0.367	0.017
0.03	0.36	0.017	0.247	0.034
0.04	0.367	0.038	0.214	0.014
0.05	0.254	0.063	0.342	0.033
0.06	0.369	0.044	0.271	0.011
0.07	0.284	0.031	0.318	0.012
0.08	0.282	0.045	0.237	0.039
0.09	0.218	0.022	0.249	0.061
0.10	0.288	0.048	0.368	0.042
0.11	0.304	0.019	0.228	0.043
0.12	0.249	0.094	0.202	0.054
0.13	0.235	0.118	0.296	0.056
0.14	0.275	0.121	0.221	0.017
0.15	0.305	0.131	0.28	0.044
0.16	0.339	0.083	0.364	0.092
0.17	0.258	0.076	0.355	0.043
0.18	0.316	0.092	0.313	0.014
0.19	0.354	0.023	0.245	0.043

References

1. Stone, R. *Introduction to Internal Combustion Engines*, 2nd ed.; Palgrave Macmillan: London, UK, 1985; pp. 23–25. ISBN 978-1-349-22147-9.
2. Guzzella, L.; Onder, C.H. *Introduction to Modeling and Control of Internal Combustion Engine Systems*; Springer: Berlin, Germany, 2010; pp. 2622–2626. ISBN 978-3-662-08003-0.
3. Taylor, A.M.K.P. Science review of internal combustion engines. *Energy Policy* **2008**, *36*, 4657–4667. [CrossRef]
4. Qiao, Y.; Huang, K.; Jeub, J.; Qian, J.; Song, Y. Deploying Electric Vehicle Charging Stations Considering Time Cost and Existing Infrastructure. *Energies* **2018**, *11*, 2436. [CrossRef]
5. Groff, E.G. *Automotive Two-Stroke-Cycle Engine Development in the 1980-1990's*; Technical Paper; SAE International: Detroit, MI, USA, 2016.
6. Krutilla, K.; Graham, J.D. Are Green Vehicles Worth the Extra Cost? The Case of Diesel-Electric Hybrid Technology for Urban Delivery Vehicles. *J. Policy Anal. Manag.* **2012**, *31*, 501–532. [CrossRef]
7. Wang, F.K.; Saito, M. Evaluating the efficiency of green vehicles and diesel vehicles. *Int. J. Green Energy* **2016**, *13*, 1163–1174. [CrossRef]
8. Haddadian, G.; Khodayar, M.; Shahidehpour, M. Accelerating the global adoption of electric vehicles: Barriers and drivers. *Electr. J.* **2015**, *28*, 53–68. [CrossRef]

9. Trigg, T.; Telleen, P.; Boyd, R.; Cuenot, F.; D'Ambrosio, D.; Gaghen, R.; Gagné, J.; Hardcastle, A.; Houssin, D.; Jones, A. Global EV outlook: Understanding the electric vehicle landscape to 2020. *Int. Energy Agency* **2013**, *1*, 1–40.
10. Reddi, K.; Elgowainy, A.; Rustagi, N.; Gupta, E. Impact of hydrogen refueling configurations and market parameters on the refueling cost of hydrogen. *Int. J. Hydrog. Energy* **2017**, *42*, 21855–21865. [CrossRef]
11. Enang, W.; Bannister, C. Modelling and control of hybrid electric vehicles (A comprehensive review). *Renew. Sustain. Energy Rev.* **2017**, *74*, 1210–1239. [CrossRef]
12. Geetha, A.; Subramani, C. A comprehensive review on energy management strategies of hybrid energy storage system for electric vehicles. *Int. J. Energy Res.* **2017**, *41*, 1817–1834. [CrossRef]
13. Tie, S.F.; Tan, C.W. A review of energy sources and energy management system in electric vehicles. *Renew. Sustain. Energy Rev.* **2013**, *20*, 82–102. [CrossRef]
14. Lim, D.J.; Jahromi, S.R.; Anderson, T.R.; Tudorie, A.A. Comparing technological advancement of hybrid electric vehicles (HEV) in different market segments. *Technol. Forecast. Soc. Chang.* **2015**, *97*, 140–153. [CrossRef]
15. Homchaudhuri, B.; Lin, R.; Pisu, P. Hierarchical control strategies for energy management of connected hybrid electric vehicles in urban roads. *Transp. Res. Part C Emerg. Technol.* **2016**, *62*, 70–86. [CrossRef]
16. Zhang, P.; Yan, F.; Du, C. A comprehensive analysis of energy management strategies for hybrid electric vehicles based on bibliometrics. *Renew. Sustain. Energy Rev.* **2015**, *48*, 88–104. [CrossRef]
17. Bayindir, K.Ç.; Gözüküçük, M.A.; Teke, A. A comprehensive overview of hybrid electric vehicle: Powertrain configurations, powertrain control techniques and electronic control units. *Energy Convers. Manag.* **2011**, *52*, 1305–1313. [CrossRef]
18. Yi, C.; Epureanu, B.I.; Hong, S.K.; Ge, T.; Yang, X.G. Modeling, control, and performance of a novel architecture of hybrid electric powertrain system. *Appl. Energy* **2016**, *178*, 454–467. [CrossRef]
19. Shabbir, W.; Evangelou, S.A. Real-time control strategy to maximize hybrid electric vehicle powertrain efficiency. *Appl. Energy* **2014**, *135*, 512–522. [CrossRef]
20. Sockeel, N.; Shi, J.; Shahverdi, M.; Mazzola, M. Pareto Front Analysis of the Objective Function in Model Predictive Control Based Power Management System of a Plug-in Hybrid Electric Vehicle. In Proceedings of the 2018 IEEE Transportation Electrification Conference and Expo (ITEC), Chicago, IL, USA, 13–15 June 2018; pp. 1–6.
21. Sockeel, N.; Shahverdi, M.; Mazzola, M. Impact of the State of Charge estimation on Model Predictive Control Performance in a Plug-in Hybrid Electric Vehicle accounting for equivalent fuel consumption and battery capacity fades. In Proceedings of the 2019 IEEE Transportation Electrification Conference and Expo (ITEC), Detroit, MI, USA, 19–21 June 2019; pp. 127–136.
22. Huang, Y.; Wang, H.; Khajepour, A.; He, H.; Ji, J. Model predictive control power management strategies for HEVs: A review. *J. Power Sources* **2017**, *341*, 91–106. [CrossRef]
23. Di Cairano, S.; Bernardini, D.; Bemporad, A.; Kolmanovsky, I.V. Stochastic MPC with learning for driver-predictive vehicle control and its application to HEV energy management. *IEEE Trans. Control Syst. Technol.* **2013**, *22*, 1018–1031. [CrossRef]
24. Yan, F.; Wang, J.; Huang, K. Hybrid electric vehicle model predictive control torque-split strategy incorporating engine transient characteristics. *IEEE trans. Veh. Technol.* **2012**, *61*, 2458–2467. [CrossRef]
25. Minh, V.; Rashid, A. Modeling and model predictive control for hybrid electric vehicles. *Int. J. Automot. Technol.* **2012**, *13*, 477–485. [CrossRef]
26. Xiang, C.; Ding, F.; Wang, W.; He, W. Energy management of a dual-mode power-split hybrid electric vehicle based on velocity prediction and nonlinear model predictive control. *Appl. Energy* **2017**, *189*, 640–653. [CrossRef]
27. Ibrahim, M.; Jemei, S.; Wimmer, G.; Hissel, D. Nonlinear autoregressive neural network in an energy management strategy for battery/ultra-capacitor hybrid electrical vehicles. *Electr. Power Syst. Res.* **2016**, *136*, 262–269. [CrossRef]
28. Paganelli, G.; Delprat, S.; Guerra, T.M.; Rimaux, J.; Santin, J.J. Equivalent consumption minimization strategy for parallel hybrid powertrains. In Proceedings of the 2002 IEEE Vehicular Technology Conference, Birmingham, AL, USA, 6–9 May 2002; pp. 2076–2081.

29. Onori, S.; Serrao, L.; Rizzoni, G. *Hybrid Electric Vehicles Energy Management Strategies*; Springer: London, UK, 2016; pp. 65–77. ISBN 978-1-4471-6781-5.
30. Teng, L.; Hu, X.; Li, S.E.; Cao, D. Reinforcement Learning Optimized Look-Ahead Energy Management of a Parallel Hybrid Electric Vehicle. *IEEE/ASME Trans. Mechatron.* **2017**, *22*, 1497–1507.
31. Alegre, S.; Míguez, J.V.; Carpio, J. Modelling of electric and parallel-hybrid electric vehicle using Matlab/Simulink environment and planning of charging stations through a geographic information system and genetic algorithms. *Renew. Sustain. Energy Rev.* **2017**, *74*, 1020–1027. [CrossRef]
32. Barth, M.; An, F.; Norbeck, J.; Ross, M. Modal emissions modeling: A physical approach. *Transp. Res. Rec.* **1996**, *1520*, 81–88. [CrossRef]
33. Cappiello, A.; Chabini, I.; Nam, E.K.; Lue, A.; Zeid, M.A. A statistical model of vehicle emissions and fuel consumption. In Proceedings of the 2002 IEEE 5th International Conference on Intelligent Transportation Systems, Singapore, 3–6 September 2002; pp. 801–809.
34. Ahn, K.; Rakha, H.; Trani, A.; Van Aerde, M. Estimating vehicle fuel consumption and emissions based on instantaneous speed and acceleration levels. *J. Transp. Eng.* **2002**, *128*, 182–190. [CrossRef]
35. Rakha, H.; Ahn, K.; Trani, A. Development of VT-Micro model for estimating hot stabilized light duty vehicle and truck emissions. *Transp. Res. Part D: Transp. Environ.* **2004**, *9*, 49–74. [CrossRef]
36. Asher, Z.; Galang, A.; Briggs, W.; Johnston, B. *Economic and Efficient Hybrid Vehicle Fuel Economy and Emissions Modeling Using an Artificial Neural Network*; Technical Paper; SAE International: Detroit, MI, USA, 2018.
37. Qiao, Y.; Duan, X.; Huang, K.; Song, Y.; Qian, J. Scavenging Ports' Optimal Design of a Two-Stroke Small Aeroengine Based on the Benson/Bradham Model. *Energies* **2018**, *11*, 2739. [CrossRef]
38. Serrao, L.; Onori, S.; Rizzoni, G. ECMS as a realization of Pontryagin's minimum principle for HEV control. In Proceedings of the 2009 IEEE American Control Conference, St. Louis, MO, USA, 10–12 June 2009; pp. 3964–3969.
39. Demuynck, J.; Bosteels, D.; De Paepe, M.; Favre, C.; May, J.; Verhelst, S. Recommendations for the new WLTP cycle based on an analysis of vehicle emission measurements on NEDC and CADC. *Energy Policy* **2012**, *49*, 234–242. [CrossRef]
40. Pavlovic, J.; Marotta, A.; Ciuffo, B. CO_2 emissions and energy demands of vehicles tested under the NEDC and the new WLTP type approval test procedures. *Appl. Energy* **2016**, *177*, 661–670. [CrossRef]
41. Pavlovic, J.; Ciuffo, B.; Fontaras, G.; Valverde, V.; Marotta, A. How much difference in type-approval CO2 emissions from passenger cars in Europe can be expected from changing to the new test procedure (NEDC vs. WLTP)? *Transp. Res. Part A Policy Pract.* **2018**, *111*, 136–147. [CrossRef]
42. Fontaras, G.; Ciuffo, B.; Zacharof, N.; Tsiakmakis, S.; Marotta, A.; Pavlovic, J.; Anagnostopoulos, K. The difference between reported and real-world CO_2 emissions: How much improvement can be expected by WLTP introduction? *Transp. Res. Procedia* **2017**, *25*, 3933–3943. [CrossRef]
43. Ciuffo, B.; Maratta, A.; Tutuianu, M.; Anagnostopoulos, K.; Fontaras, G.; Pavlovic, J.; Serra, S.; Tsiakmakis, S.; Zacharof, N. Development of the Worldwide Harmonized Test Procedure for Light-Duty Vehicles: Pathway for Implementation in European Union Legislation. *Transp. Res. Rec.* **2015**, *2503*, 110–118. [CrossRef]
44. Mera, Z.; Fonseca, N.; López, J.M.; Casanova, J. Analysis of the high instantaneous NOx emissions from Euro 6 diesel passenger cars under real driving conditions. *Appl. Energy* **2019**, *242*, 1074–1089. [CrossRef]
45. Suarez-Bertoa, R.; Astorga, C. Impact of cold temperature on Euro 6 passenger car emissions. *Environ. Pollut.* **2018**, *234*, 318–329. [CrossRef] [PubMed]
46. Zhang, S.; Wu, Y.; Wu, X.; Li, M.; Ge, Y.; Liang, B.; Xu, Y.; Zhou, Y.; Liu, H.; Fu, L. Historic and future trends of vehicle emissions in Beijing, 1998–2020: A policy assessment for the most stringent vehicle emission control program in China. *Atmos. Environ.* **2014**, *89*, 216–229. [CrossRef]
47. Wu, X.; Wu, Y.; Zhang, S.; Liu, H.; Fu, L.; Hao, J. Assessment of vehicle emission programs in China during 1998–2013: Achievement, challenges and implications. *Environ. Pollut.* **2016**, *214*, 556–567. [CrossRef] [PubMed]
48. Wahl, H.G.; Gauterin, F. An Iterative Dynamic Programming Approach for the Global Optimal Control of Hybrid Electric Vehicles under Real-time Constraints. In Proceedings of the 2013 IEEE Intelligent Vehicles Symposium, Gold Coast City, Australia, 23–26 June 2013; pp. 592–597.

49. Lian, H.; Zeng, C.; Cai, Z. Dynamic programming based optimal control strategy of the hybrid vehicular power system. In Proceedings of the 2017 43rd Annual Conference of the IEEE Industrial Electronics Society, Beijing, China, 29 October–1 November 2017; pp. 7123–7127.
50. Ozatay, E.; Onori, S.; Wollaeger, J.; Ozguner, U.; Rizzoni, G.; Filev, D.; Michelini, J.; Cairano, S.D. Cloud-Based Velocity Profile Optimization for Everyday Driving: A Dynamic-Programming-Based Solution. *IEEE Trans. Intell. Transp. Syst.* **2014**, *15*, 2491–2505. [CrossRef]